Comparison of basin-scale *in situ* and meteoric [10]Be erosion and denudation rates across a rainfall, slope, and elevation gradient at George River, northeast Tasmania, Australia

Leah VanLandingham[1], Eric W. Portenga[1], Edward C. Lefroy[2], Paul R. Bierman[3], Alan J. Hidy[4]

[1]Geography and Geology Department, Eastern Michigan University, Ypsilanti, MI 48197, United States
[2]Tasmanian Institute of Agriculture, University of Tasmania, Private Bag 98, Hobart 7001, Australia
[3]Rubenstein School for Natural Resources and the Environment, University of Vermont, Burlington, VT 05405, United States
[4]Center for Accelerator Mass Spectrometry, Lawrence Livermore National Laboratory, Livermore, CA 94550, United States

Correspondence to: Eric W. Portenga (eric.portenga@emich.edu), Paul R. Bierman (paul.bierman@uvm.edu)

Abstract. Long-term erosion rates in Tasmania, at the southern end of Australia's Great Dividing Range, are poorly known, yet such knowledge is critical for making informed land-use decisions and improving ecological health of coastal ecosystems. Here, we present the first quantitative, geologically-relevant estimates of erosion rates for the George River basin, in northeast Tasmania, based on in-situ produced [10]Be ($^{10}Be_i$) measured from stream sand at two trunk channel sites and seven tributaries (average 10.5 mm kyr^{-1}). These new $^{10}Be_i$-based erosion rates are strongly related to mean annual precipitation rates and elevation, and we suggest that the current East-West precipitation gradient across George River greatly influences erosion in northeast Tasmania. This stands in contrast to erosion rates along the mainland portions of Australia's Great Dividing Range, which are more strongly related to basin slope. We also extract and measure meteoric [10]Be ($^{10}Be_m$) from sediment grain coatings of the stream sand at each site, which we use to estimate $^{10}Be_m$-based erosion and denudation rates for George River. $^{10}Be_m$ based erosion and denudation metrics, particularly those from the central and eastern tributaries, are also closely related to elevation and precipitation in the same manner as $^{10}Be_i$ erosion rates. Although $^{10}Be_m$-based denudation rates replicate $^{10}Be_i$ erosion rates within a factor of two, $^{10}Be_m$-based erosion rates are systematically 5–6x higher than $^{10}Be_i$ erosion rates. $^{10}Be_m$ erosion and denudation metrics for the westernmost headwater catchments are significantly lower than expected and have likely been affected by intensive and widespread topsoil erosion related to forestry, which delivers large volumes of sediment rich in $^{10}Be_m$ to tributary streams. The $^{10}Be_i$ erosion rates presented in this study may be useful for land managers seeking to restore ecological health of Tasmania's estuaries by reducing sediment input to levels prior to landscape disturbance.

1 Introduction

Erosion rates of river basins derived from measurements of the in-situ produced cosmogenic isotope, $^{10}Be_i$, have been used to elucidate and infer topographic, tectonic, and climate drivers of landscape evolution for thousands of individual river basins (Codilean et al., 2018; Harel et al., 2016; Mishra et al., 2019; Portenga and Bierman, 2011; Wittmann et al., 2020). Recently, erosion rates from individual studies have been compiled and analyzed at the scale of entire continental orogens to demonstrate

primary and secondary controls on erosion across thousands to tens of thousands of years (Aguilar et al., 2014; Carretier et al., 2018; Codilean et al., 2021; Delunel et al., 2020; Starke et al., 2020). For example, Delunel et al. (2020) find that $^{10}Be_i$ erosion rates across the European Alps are strongly linked to mean basin slope and influenced by uplift and glaciations. A number of

35   north-south latitudinal studies from the South American Andes show that some segments of the range are driven by uplift (Carretier et al., 2015; Starke et al., 2017) and slope (Carretier et al., 2018) but not necessarily rainfall unless one considers the effects of vegetation in driving soil weathering rates (Carretier et al., 2015; Starke et al., 2020).

A new compilation and analysis of $^{10}Be_i$ erosion rates across the Great Dividing Range on eastern Australia, however, is the

40   first to analyze landscape dynamics across a continent-spanning, passive, post-orogenic rift margin and finds that basin slope is most closely related to erosion at all spatial scales, more so than any other potential driver of erosion (Codilean et al., 2021). While Codilean et al.'s (2021) analysis comprises erosion rates from the Western and Eastern flanks of the Great Dividing Range – northern tropics to temperate southeast Australia – it is restricted to mainland Australia.

Here, we supplement Codilean et al.'s (2021) study with the first $^{10}Be_i$-based erosion rates from the southernmost end of the

45   eastern Australian passive margin on the island-state of Tasmania and the first presented for temperate rainforests in the Southern Hemisphere (Fig. 1; cf. Adams and Ehlers, 2017; Belmont et al., 2007). Furthermore, important quantitative erosion rate data for Tasmania and many of its fluvial systems are currently lacking (Jerie et al., 2003; Koehnken, 2001), and providing new erosion rate data will provide useful information for land managers and estuary restoration efforts.
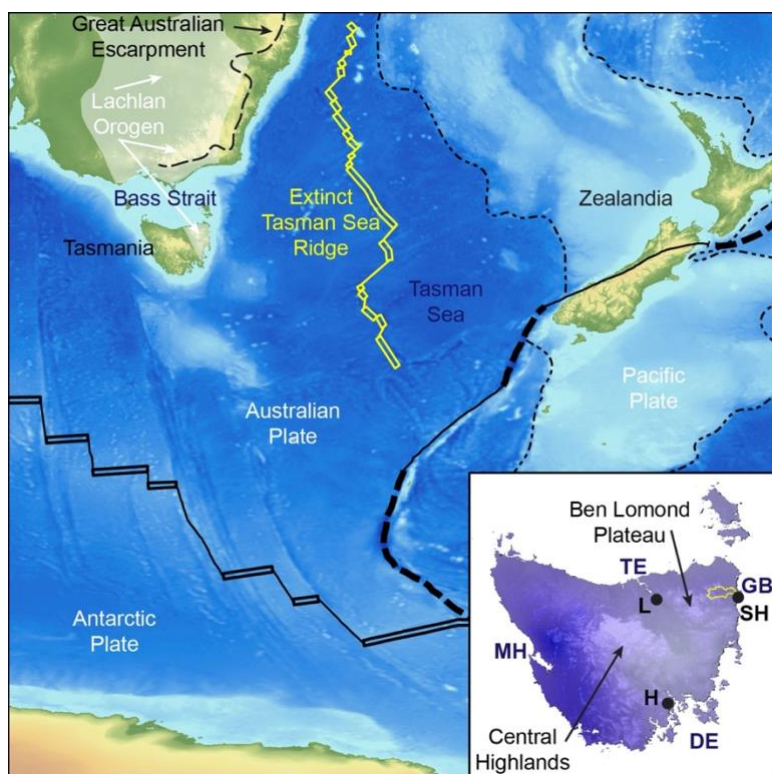
Figure 1: Generalized tectonic map of the eastern Southern Ocean/southwest Pacific Ocean, surrounding Tasmania, including large-scale geologic structures in southeast Australia and Tasmania. Inset shows normalized island-wide precipitation gradient across Tasmania with darker shades of blue being areas with more precipitation. The Central Highlands establishes a pronounced rainfall shadow on the east side of the island. The Ben Lomond Plateau promotes a secondary, more-localized East-West precipitation gradient for northeast Tasmania where the field area for this study is located; the main George River basin is shown outlined in yellow. Major estuaries are indicated: Derwent Estuary (DE), Macquarie Harbour (MH), Tamar Estuary (TE), Georges Bay (GB). Cities are shown with black dots for reference: Hobart (H), Launceston (L), St. Helens (SH).

50

1.1 Importance of Erosion of George River and the Georges Bay Watershed

Applications of $^{10}Be_i$ erosion studies in Australia often are set within the context of assessing the impact of sediment delivery to sensitive offshore coastal environments, primarily the Great Barrier Reef (Croke et al., 2015; Nichols et al., 2014). Recently, efforts to conserve and restore estuarine environments across Australia have gained significant traction, particularly because

55 estuaries link terrestrial fluvial systems to coastal environments and act as a biogeochemical buffer and sediment trap between the two environments (Creighton et al., 2015; Fitzsimmons et al., 2015; Wolanski and Ducrotoy, 2014). These restoration efforts include hundreds of Tasmanian estuaries (Coughanowr and Whitehead, 2013; Edgar et al., 2000; Murphy et al., 2003), which suffer from centuries of human-caused degradation resulting from urbanization, introduction of invasive species, forestry, mining, fishing, agriculture, and tourism (Augustineus et al., 2010; Butler, 2006; Davis and Kidd, 2012; Edgar and

60 Barrett, 2000; Ellison and Sheehan, 2014; Jones et al., 2003; Martin-Smith and Vincent, 2005; Nanson et al., 1994; Seen et al., 2004). Active conservation, restoration, and monitoring efforts are underway at many Tasmanian estuaries (Beard et al., 2008; Crawford and White, 2005; Creighton et al., 2015); none quantify geologically-relevant erosion rates nor sediment delivery, despite a recognized need to lower sediment delivery in order to reduce nutrient and pollutant loads, improve water clarity, and prevent burial of hard surfaces important for marine life (Elliott et al., 2007; Geist and Hawkins, 2016; Noe et al.,

65 2020; Verdonschot, 2013).

This study focuses on the Georges Bay estuary in northeast Tasmania, which is known for its oyster stocks (Mitchell et al., 2000) but has been degraded by a history of timber production, tin mining, and agriculture. Historical land-use practices have supplied >10^6 m^3 of sediment to Georges Bay's primary tributary, the George River (no "s"), since the late 19th century

70 (Knighton, 1991) and continue to supply pollutants to Georges Bay (Bleaney et al., 2015; Crawford and White, 2005). The intensive historical industrial use of the land in the George River catchment and the threat of excess sediment delivery to the fragile estuarine environment in Georges Bay has driven state and local municipalities to focus restoration and conservation efforts on the bay. As elsewhere, the success of these efforts relies in part, on reducing sediment delivery from George River to Georges Bay (Batley et al., 2010; Crawford and White, 2005; Kragt and Newham, 2009; McKenny and Shepherd, 1999;

75 Mount et al., 2005).

1.2 *In situ* ^{10}Be and meteoric ^{10}Be erosion and denudation metrics

The primary goal of this study is to provide background rates (over millennia) of landscape change and sediment delivery from the George River to Georges Bay using the *in situ* cosmogenic isotope beryllium-10 ($^{10}Be_i$) in fluvial sediment (Bierman and

80 Steig, 1996; Brown et al., 1995; Granger et al., 1996). $^{10}Be_i$ production decreases exponentially with depth in rock and sediment at Earth's surface such that $^{10}Be_i$ concentrations at depths >2 m is negligible compared to that measured closer to Earth's surface (Gosse and Phillips, 2001; Lal, 1991); $^{10}Be_i$ produced by muons dominates at depths >2 m (Braucher et al., 2003; Gosse and Phillips, 2001; Heisinger et al., 1997), but muogenic $^{10}Be_i$ production is generally negligible when compare to

spallogenic $^{10}Be_i$ production, except in rapidly eroding landscapes or landscapes with steep terrain (e.g. Dethier et al., 2014;
85   Fellin et al., 2017; Rosenkranz et al., 2018; Scherler et al., 2014; Siame et al., 2011) or in paleoerosion studies (e.g. Schaller
et al., 2001, 2004, 2016). Bioturbation homogenizes $^{10}Be_i$ concentrations in soils (Brown et al., 1995; Granger et al., 1996;
Schaller et al., 2018), and $^{10}Be_i$ erosion rates are therefore considered to be insensitive to widespread shallow erosion. This
insensitivity allows $^{10}Be_i$ erosion rates to be a useful gauge of pre-disturbance rates of landscape change (Ferrier et al., 2005;
Portenga et al., 2019; Schmidt et al., 2018; Vanacker et al., 2007); exceptions have been noted where human land use is
90   intensive (i.e. Schmidt et al., 2016) or the effects of human land use are exacerbated by climate extremes (i.e. Rosenkranz et
al., 2018). Pre-disturbance $^{10}Be_i$ erosion data can inform approaches to reducing sediment delivery from George River and
support efforts to improve the ecological health of Georges Bay estuary and possibly other watersheds in northeast Tasmania
that share similar bedrock and topographic characteristics.

95   Whereas $^{10}Be_i$ is produced in rock and sediment, ^{10}Be is also produced via spallation of oxygen in the atmosphere; this ^{10}Be
rains out or falls to Earth's surface (meteoric ^{10}Be; $^{10}Be_m$) where it is readily adsorbed into sediment grain coatings and
traditionally used to trace sediment through landscapes (Brown et al., 1988; Heikkilä and von Blanckenburg, 2015; Helz et al.,
1992; Monaghan et al., 1986; Portenga et al., 2017; Reusser et al., 2010b; Valette-Silver et al., 1986). Recently derived
equations allow erosion rates and denudation rates to be calculated from measurements of $^{10}Be_m$ and the chemically-similar,
100 non-cosmogenic ^9Be, which is weathered out of mineral grains ($^9Be_{reac}$; Willenbring and von Blanckenburg, 2010; von
Blanckenburg et al., 2012). $^{10}Be_m$ erosion and $^{10}Be_m/^9Be_{reac}$ denudation rates have been used to quantify landscape evolution
over a variety of spatial scales for long-established river basins (Dannhaus et al., 2018; Deng et al., 2020; Harrison et al., 2021;
Portenga et al., 2019; Rahaman et al., 2017; Wittmann et al., 2012, 2015) and has shown particular promise in quantifying
landscape dynamics in quartz-poor landscapes (Deng et al., 2020; Rahaman et al., 2017).

105

Here, we consider erosion to be the physical mass loss from a landscape and denudation to be the sum of physical and chemical
mass loss. Conceptually, and with regards to ^{10}Be, Portenga et al. (2019) suggested that if soil thickness approximates the zone
of $^{10}Be_i$ production (<2 m) and if pH values in the environment are high (>3.9, Graly et al., 2010) such that no $^{10}Be_m$ desorbs
from sediment grain coatings, erosion and denudation rates derived from measurements of $^{10}Be_i$ and $^{10}Be_m/^9Be_{reac}$ should be
110 comparable and should measure landscape dynamics similarly. Although replication between $^{10}Be_i$ and $^{10}Be_m$ erosion and
denudation rates at individual sites is poor (Portenga et al., 2019; Rahaman et al., 2017; Wittmann et al., 2015), average rates
from $^{10}Be_i$ and $^{10}Be_m/^9Be_{reac}$ erosion and denudation datasets tend to be similar in magnitude, and similar spatial patterns of
landscape change emerge from both $^{10}Be_i$ and $^{10}Be_m$ datasets across large regions (Deng et al., 2020; Portenga et al., 2019;
Wittmann et al., 2015). Further use of the $^{10}Be_m/^9Be_{reac}$ denudation method in landscapes where $^{10}Be_i$ erosion can be measured
115 and compared is important for evaluation the veracity of $^{10}Be_m$ erosion and $^{10}Be_m/^9Be_{reac}$ denudation calculations.

The small size and relatively uniform bedrock geology of George River basin provide an ideal location to compare $^{10}Be_i$ erosion rates with erosion and denudation rates derived using $^{10}Be_m$ and $^{10}Be_m/^9Be_{reac}$, respectively (Willenbring and von Blanckenburg, 2010; von Blanckenburg et al., 2012); additionally, measured soil pH values in the catchment range from 4.0–

120   5.5 (Kidd et al., 2015), thereby suggesting that $^{10}Be_m$ loss to chemical weathering is not a concern in George River. Thus, a secondary goal of this study is to compare $^{10}Be_m$ erosion and denudation rates to $^{10}Be_i$ erosion rates as a means of assessing the efficacy of the $^{10}Be_m$ erosion and $^{10}Be_m/^9Be_{reac}$ denudation methods in a landscape that minimizes geological heterogeneity, which otherwise may introduce scatter to larger datasets covering larger, more geologically-diverse landscapes (i.e. Deng et al., 2020; Portenga et al., 2019; Rahaman et al., 2017). Although George River has a simple bedrock geology, it also has a

125   long history of intensive lode and placer tin mining that has, in the past, disturbed its fluvial systems (Knighton, 1991; Preston, 2012). Given that intensive land-use histories have affected results of $^{10}Be_m$ calculations elsewhere (Portenga et al., 2019), we explore how mining in George River affects our interpretations of ^{10}Be-based erosion and denudation calculations throughout this study.

Figure 2: A. Shaded relief map of the topography of George River basin. Areas of historic mining are shown (Knighton, 1991), the action of which delivered >10⁶ m³ to the George River delta in Georges Bay (GB). B. Bedrock geology map of George River shows the widespread occurrence of Devonian felsic intrusions of the Blue Tier Batholith, which underlies the vast majority of the field area. Note that basins TG-2, TG-4, TG-5, and TG-8 are almost entirely underlain by

130

2 Field Area

Tasmania separated from mainland Australia during Cretaceous rifting of Antarctica and Australia and sits at the southern end of the Great Australian Escarpment – a steep arch-type escarpment that formed during the separation of Zealandia from
135 mainland Australia in the Mid- to Late-Cretaceous (Fig. 1; Codilean et al., 2021; Crowder et al., 2019; Etheridge et al., 1987; Gaina et al., 1998; Griffiths, 1971; Gunn, 1975; Hayes and Ringis, 1973; Lanyon et al., 1993; Matmon et al., 2002; McDougall and van der Lingen, 1974; Mortimer et al., 2017; Persano et al., 2002; Sutherland et al., 2001; Weissel and Hayes, 1977). Bedrock of George River basin comprises granodiorite and granite associated with the Blue Tier Batholith, which were contemporaneously emplaced into sediments of the Mathinna Supergroup in the Devonian (Fig. 2; Foster et al., 2000; Gee and
140 Groves, 1971; Gray and Foster, 2004; Higgins et al., 1985; McCarthy and Groves, 1979; Seymour et al., 2006). Siluro-Devonian sedimentary rocks and Neogene basalts underlie small areas, primarily along drainage divides in the central and western George River basin (Seymour et al., 2006).
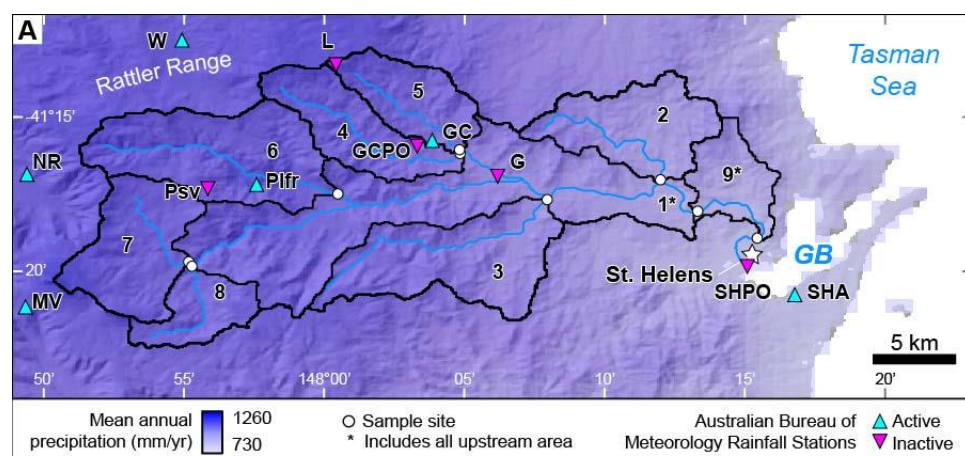
Figure 3: A. Mean annual precipitation across George River basin in northeast Tasmania exhibiting East-West precipitation gradient. **B.** Mean annual precipitation from the WorldClim global dataset (Fick and Hijmans, 2017) and elevation across George River basin binned at 01' longitudinal intervals. **C.** Logarithmic relationship between mean annual precipitation and elevation; data points binned at 01' longitudinal intervals. Historic rainfall data from active and inactive rainfall gaging stations (cyan and magenta triangles, respectively; BoM, 2021) is greater than modeled WorldClim rainfall for comparable elevations (Table 1), but the overall relationship between elevation and rainfall persists, regardless of which rainfall data are used.
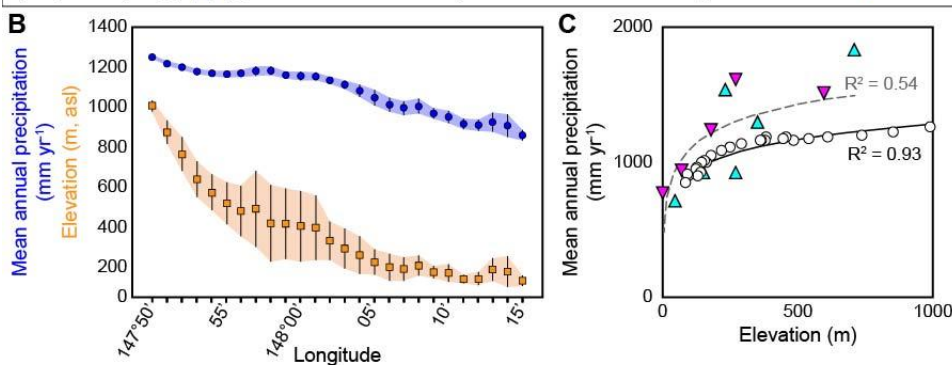
145 George River basin is of modest size (557 km^2) in northeastern Tasmania with low elevation (mean = 386 m) and gentle hillslopes (mean = 10°) that drain the eastern slopes of the Rattler Range, which currently has a warm, temperate climate (Kottek et al., 2006). Despite eastern Tasmania being in the rain shadow of the central Tasmanian Highlands and western coast

ranges, the local topography of the Ben Lomond Plateau induces a moderate east-west precipitation gradient across George
River basin (1,261–970 mm yr^{-1}; Fig. 3; Table 1; BoM, 2021; Fick and Hijmans, 2017).

150

	Table 1. Sample locations and basin data						
Sample ID	Sample Location			Elevation (m)[a]	Basin Area (km²)[a]	Relief (m)[a]	Mean weighted slope (°)[a]	Mean annual precipitation (mm yr⁻¹)[b]
	River name	Latitude (°)	Longitude (°)					
TG-1	George River	-41.29017	148.22217	346	397.25	1127	10	1122
TG-2	Forester Creek	-41.27183	148.19925	141	40.21	298	6	970
TG-3	Powers Creek	-41.28286	148.13247	265	55.56	670	10	1065
TG-4	Groves Creek	-41.25514	148.08317	364	34.39	776	11	1161
TG-5	Ransom River	-41.25364	148.08239	347	27.71	709	10	1168
TG-6	North George River	-41.28067	148.00697	439	65.84	790	12	1211
TG-7	South George River	-41.32208	147.92172	652	42.53	753	9	1261
TG-8	Mt. Albert Rivulet	-41.32178	147.92592	596	20.42	631	10	1206
TG-9	George River @ St. Helens	-41.31350	148.26531	331	426.88	1174	10	1107

[a] Based or derived from Satellite Radar Topography Mission data, 90 m resolution (Gallant et al., 2011)
[b] Rainfall data are modelled precipitation rates from the WorldClim dataset, 1 km² resolution (Fick and Hijmans, 2017)

Aboriginal Australians crossed to Tasmania from mainland Australia >35 ka (Cosgrove, 1995; Cosgrove et al., 1990), possibly
corresponding to subaerial exposure of the Bass Strait ~56–40 ka (McIntosh et al., 2006) and localized ice advances in the
155 central Tasmanian highlands (Barrows et al., 2001, 2002; Macintosh et al., 2006). Ecological habitat suitability models, based
on characteristics and locations of thousands of archaeological sites across Tasmania indicate that Aboriginal communities
were located close to freshwater sources and coastal resources, such as the landscapes around Georges Bay and the lower
elevations within George River tributaries (Jones et al., 2019). Human arrival in Tasmania has been linked to widespread
erosion events in mid-elevation landscapes (McIntosh et al., 2009).

160

Historically, decades of intensive tin lode mining in isolated headwaters of some tributaries and pockets of hydraulic sluice
mining for tin in lowland floodplains introduced >10^6 m^3 of tailings to George River and its tributaries (Fig. 2a), decreasing
the average grain size of alluvium from 30–50 mm to 1–2 mm (Knighton, 1991). Bedload characteristics have since returned
to pre-disturbance levels following widespread alluvium storage in floodplains and aggradation at the George River delta in
165 Georges Bay (Knighton, 1991; Cheetham and Martin, 2018). Despite George River's return to pre-disturbance channel and
bedload characteristics, a study from an experimental forest in the Gentle Annie tributary to George River shows that sediment
yields from logged plots relative to unlogged plots continues to contribute sediment to the George River system (Wilson,
1999). More recently, land use within George River basin in 2008, at the time of sample collection, consisted primarily of
forestry production from relatively natural environments and secondarily of conservation land (Fig. 4); intensive land use (i.e.
170 built structures, permanent land alteration) and agricultural production from unirrigated land occur in equal proportion, though
much less than the primary and secondary land uses; a small percentage of George River is used for agricultural production
from irrigated lands (ABARES, 2016).
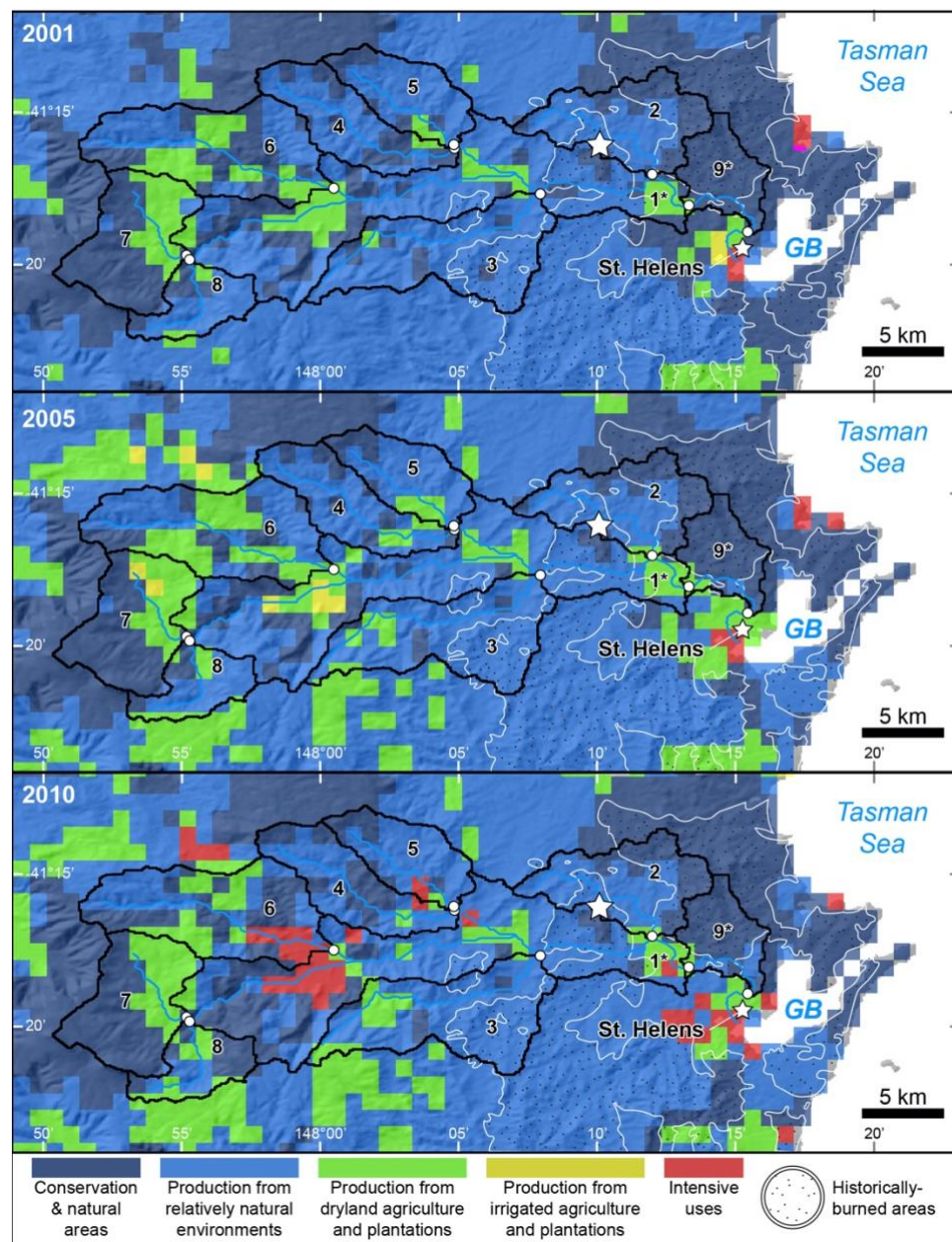
Figure 4: Land cover for each sampled tributary catchment in George River basin from 2001 (top), 2005 (center), and 2010 (bottom) – the period of leading up to and immediately following sample collection in 2008. The Australian Land Use and Management Classification system groups land use into five primary Classes based on their potential to impact the natural environment (ABARES, 2016). White star denotes location of the Gentle Annie experimental catchment (Wilson, 1999). Stippled areas outlined in white are areas that have been affected by forest fires or prescribed burns in the past (Land Tasmania, 2020). Asterisk (*) indicates trunk channel catchments.

175

3 Methods

Sediment samples for this study were collected in 2008 from several locations along the trunk ($n = 2$) and tributaries ($n = 7$) of George River (Fig. 2). At each site, sediment was collected from the streambed and/or in-channel bars to ensure active fluvial transport and mixing. Samples were sieved in the field to the 250–850 μm grain-size fraction. Although this grain-size

180 is finer than the mean natural grain size (30–50 mm; Knighton, 1991), previous studies show that $^{10}Be_i$ grain-size bias is minimal or not present in small, low-elevation, low-relief, temperate landscapes where landslides are uncommon (van Dongen

et al., 2019); thus, $^{10}Be_i$ measured from the 250–850 μm grain-size fraction can be interpreted as geological erosion rates. $^{10}Be_m$ and the weathered and *in situ* phases of ^9Be ($^9Be_{reac}$, $^9Be_{min}$, respectively) were measured from the 250–850 μm grain-size fraction from all seven tributary sites and one of the trunk channel sites.

185

$^{10}Be_i$ was extracted from quartz from each sample at the University of Vermont following standard methods, during which a known amount of a ^9Be carrier ($^9Be_{carr}$) was added to each sample (Kohl and Nishiizumi, 1992; Corbett et al., 2016); no native beryllium was detected in quartz concentrates from any sample, which can otherwise lead to significant overestimates of $^{10}Be_i$-based erosion rates (Portenga et al., 2015). $^{10}Be_i/^9Be_{carr}$ ratios were measured by accelerator mass spectrometry at the Lawrence

190   Livermore National Laboratory CAMS facility (Table 2); $^{10}Be_i$ measurements were blank-corrected (the average ratio of three blanks was subtracted from the ratio of unknown sample) and normalized to the 07KNSTD3110 AMS ^{10}Be standard material, which has a nominal $^{10}Be/^9Be$ ratio of 2.85 x 10^{-12} (Nishiizumi et al., 2007). $^{10}Be_i$ production was averaged across all sampled basins to a single point following Portenga and Bierman (2011), and the CRONUS on-line erosion rate calculator (Balco et al., 2008) was used to derive $^{10}Be_i$ erosion rates following the Lal (1991) and Stone (2000) scaling schemes (ε, Table 3); here,

195   ε is presented in units of mm kyr^{-1}. As in Portenga et al. (2019), we present $^{10}Be_i$-based sediment flux rates in this study (Appendix A), which we present as the factor of ε and ρ in units of Mg km^{-2} yr^{-1}, so as to compare to $^{10}Be_m/^9Be_{reac}$-based denudation rates (see below). Muogenic production of $^{10}Be_i$ is incorporated into $^{10}Be_i$ based erosion rates; however, muogenic $^{10}Be_i$ is negligible relative to spallogenic $^{10}Be_i$ production given George River's post-orogenic, low-elevation, low-relief setting.

Table 2. Isotope data

In situ Sample ID	UVM Batch No.	Quartz mass (g)	Carrier mass (μg)	LLNL Sample ID	$^{10}Be_i/^9Be_{carr}$	± 1σ	$^{10}Be_i$ (atoms g^{-1})	± 1σ
TG-1	432[a]	20.099	250.791	BE28820	4.37E-13	7.83E-15	3.64E+05	6.52E+03
TG-2	438[b]	20.100	249.506	BE29129	6.83E-13	9.31E-15	5.66E+05	7.72E+03
TG-3	438	22.423	249.704	BE29130	4.79E-13	1.41E-14	3.97E+05	1.17E+04
TG-4	438	19.288	248.814	BE29131	3.10E-13	8.41E-15	2.56E+05	6.95E+03
TG-5	438	20.702	250.296	BE29133	4.37E-13	1.02E-14	3.63E+05	8.48E+03
TG-6	446[c]	20.532	249.209	BE29303	2.81E-13	6.11E-15	2.33E+05	5.05E+03
TG-7	446	20.156	249.111	BE29304	2.28E-13	6.76E-15	1.88E+05	5.60E+03
TG-8	446	20.747	249.704	BE29305	2.99E-13	7.35E-15	2.48E+05	6.10E+03
TG-9	446	20.169	250.791	BE29306	4.94E-13	1.19E-14	4.11E+05	9.92E+03

Meteoric Sample ID	UVM Batch No.	Sample mass (g)	Carrier mass (μg)	LLNL Sample ID	$^{10}Be_m/^9Be_{carr}$	± 1σ	Q toms cm^{-2} yr	$^{10}Be_{met}$ (atoms g^{-1})	± 1σ	$^9Be_{min}$ (atoms g^{-1})	$^9Be_{reac}$ (atoms g^{-1})
TG-2	MB-15[d]	0.463	328.71	BE27783	1.51E-12	2.07E-14	8.12E+05	7.16E+07	9.83E+05	2.51E+16	1.32E+16
TG-3	MB-15	0.497	298.02	BE27784	1.50E-12	2.26E-14	8.92E+05	5.99E+07	9.05E+05	3.19E+16	1.06E+16
TG-4	MB-15	0.457	296.04	BE27785	1.12E-12	1.55E-14	9.73E+05	4.84E+07	6.69E+05	3.29E+16	1.08E+16
TG-5	MB-15	0.491	300.00	BE27786	1.05E-12	1.46E-14	9.79E+05	4.29E+07	5.95E+05	2.84E+16	1.09E+16
TG-6	MB-15	0.466	300.99	BE27787	4.30E-12	5.79E-14	1.01E+06	1.85E+08	2.50E+06	4.54E+16	4.06E+16
TG-7	MB-15	0.487	299.01	BE27788	5.60E-12	6.09E-14	1.06E+06	2.30E+08	2.50E+06	3.09E+16	5.82E+16
TG-8	MB-15	0.487	300.00	BE27789	5.35E-12	5.83E-14	1.01E+06	2.20E+08	2.40E+06	2.71E+16	5.54E+16
TG-9	MB-15	0.541	299.01	BE27790	1.19E-12	1.64E-14	9.28E+05	4.39E+07	6.06E+05	1.53E+16	1.08E+16

[a] In situ Batch 432 Blank $^{10}Be_i/^9Be_{carr}$ ratio = 1.25 x 10^{-14} ± 5.87 x 10^{-16}
[b] In situ Batch 438 Blank $^{10}Be_i/^9Be_{carr}$ ratio = 1.22 x 10^{-14} ± 1.82 x 10^{-15}
[c] In situ Batch 446 Blank $^{10}Be_i/^9Be_{carr}$ ratio = 1.27 x 10^{-14} ± 6.70 x 10^{-16}
[d] Meteoric Batch MB-15 Blank $^{10}Be_m/^9Be_{carr}$ ratio = 1.65 x 10^{-14} ± 1.72 x 10^{-15}

200

Table 3. Erosion and denudation rates								
Sample ID	ε^a (mm kyr^{-1})	± 2σ	Integration duration (kyr)	Sed Flux (Mg km^{-2} yr^{-1})	± 2σ	E (mm kyr^{-1})	± 2σ	D_m (Mg km^{-2} yr^{-1})	± 2σ
TG-1	9.6	1.6	61.8	25.9	4.3				
TG-2	4.8	0.8	122.5	13.1	2.2	42.8	0.6	26.0	0.7
TG-3	8.1	1.4	73.7	21.7	3.8	56.2	0.8	37.9	1.1
TG-4	14.1	2.4	42.1	38.1	6.5	75.9	1.0	52.6	1.5
TG-5	9.6	1.6	62.0	25.8	4.4	86.1	1.2	53.7	1.5
TG-6	16.7	2.8	35.5	45.1	7.5	20.7	0.3	28.2	0.8
TG-7	24.5	4.2	24.2	66.2	11.3	17.4	0.2	24.5	0.5
TG-8	17.6	3.0	33.7	47.5	8.0	17.3	0.2	22.7	0.5
TG-9	8.3	1.4	71.5	22.4	3.8	79.8	1.1	33.0	0.9

^{a} $^{10}Be_i$ erosion rates calculated using the CRONUS erosion rate calculator version 3.0, wrapper version 3.0 erates version 3.0, muons version 3.1 (Balco et al., 2008)

$^{10}Be_m$ was extracted following Stone's (1998) fusion method and a ^9Be carrier solution was added to each sample. $^{10}Be_m/^9Be_{carr}$ ratios of these fusion extracts were measured at the Lawrence Livermore National Laboratory CAMS facility, blank-corrected
205 (ratio of one blank was subtracted from ratio of unknown samples; Table 2) and normalized to the 07KNSTD3110 standard material (Nishiizumi et al., 2007). Sample material used to calculate $^9Be_{reac}$ was first subject to strong acid leaching to remove sediment grain coatings (Greene, 2016; Portenga et al., 2019 supplement); it was then fully digested in HF and $^9Be_{min}$ was measured in that solution. Both $^9Be_{reac}$ from sediment grain coatings and $^9Be_{min}$ from the remaining mineral material were measured by inductively coupled plasma-optical emission spectrometry (ICP-OES) at the University of Vermont. In this study,
210 E and D_m are presented in units of mm kyr^{-1} and Mg km^{-2} yr^{-1}, respectively.

E and D_m presented in this study (Table 3) are calculated using values of Q that range from 8.12 x 10^5 atoms cm^{-2} yr^{-1} to 1.06 x 10^6 atoms cm^{-2} yr^{-1} (Appendix A; Graly et al., 2011). Values of Q used here are of the same order of magnitude as $^{10}Be_m$ accumulation rates measured from a similar latitude in New Zealand (1.68 to 1.72 x 10^6 atoms cm^{-2} yr^{-1}; Reusser et al., 2010a),
215 those integrated throughout the Holocene (1.0–1.5 x 10^6 atoms cm^{-2} yr^{-1}; Heikkilä and von Blanckenburg, 2015), and atmospheric-depth integrated rates of Q (~7 x 10^5 atoms cm^{-2} yr^{-1}; Masarik and Beer, 2009; Willenbring and von Blanckenburg, 2010). We choose to use Graly et al.'s (2011) approach to deriving values of Q for this study since they are specific to the latitude and rainfall for each basin.

220 We compare ε, sediment flux, E, and D_m to various topographic and climatic factors to assess dominant processes driving or related to background landscape evolution in George River (Table 1). Topographic data are derived from the SRTM 90-m resolution global dataset (Gallant et al., 2011). We use mean annual precipitation data from the updated WorldClim global dataset instead of precipitation from meteorological stations because of its greater spatial coverage, but we note that while WorldClim rainfall values are nominally lower than measured precipitation, both datasets show increased rainfall at higher
225 elevations (Fig. 3c; BoM, 2021). Ratings of soil erosivity have been derived for Tasmania (Kidd et al., 2014, 2015) and are strongly tied to hillslope angle within George River basin (Fig. 5); thus, comparing erosion and denudation metrics against

basin slope metrics provides an adequate assessment of whether models of hillslope erodibility influences erosion in George River.

4 Results

4.1 ^{10}Be$_i$ erosion rates, ε

Erosion rates, ε, based on measured concentrations of in situ ^{10}Be (Table 3) range from 4.8 to 24.5 mm kyr^{-1} (Appendix A), and we find that the average ε from tributaries (13.6 ± 1.0 mm kyr^{-1}; 2σ) is greater than either of the trunk channel samples (TG-1 = 9.6 ± 1.6 mm kyr^{-1}; TG-9 = 8.3 ± 1.4 mm kyr^{-1}; 2σ). Tributary values for ε, and ε-based sediment flux rates are greater in the high-elevation, western headwaters of George River basin and decrease systematically, eastwards towards the lower-elevation coast (Fig. 6). This eastward decrease in ε also corresponds to a decrease in rainfall along the precipitation gradient (R^2 = 0.82); relationships between ε and basin relief, basin-weighted slope, and the percent of each basin that is categorized as being greater than or equal to High Erosivity are weak (Fig. 7; R^2 = 0.39, R^2 = 0.17, R^2 = 0.05, respectively).

Taking the product of ε and the area of each catchment provides the average annual volume of sediment exported from each catchment over millennia. Summing these volumes, shows that a similar volume of sediment passes through the trunk channel sample sites annually as the sum of sediment exiting sampled tributaries (TG-1 = 3.8 ± 0.7 km^3 yr^{-1}; TG-9 = 3.5 ± 0.7 km^3 yr^{-1}; tributaries = 3.9 ± 0.3 km^3 yr^{-1}; 2σ). Trunk channel samples, TG-1 and TG-9, should also incorporate erosion from their respective subcatchments – the area upstream of the sample site, but downstream of all tributary sample points. Using regression equations for ε and longitude, elevation, and precipitation, each, an average modelled ε for TG-1 is 9.6 ± 3.0 mm kyr^{-1} and an average modelled ε for TG-9 is 1.1 ± 3.1 mm kyr^{-1}. The average volume of sediment these subcatchments contribute to annual sediment loads, based on modelled ε data are TG-1 = 1.1 ± 0.4 km^3 yr^{-1} and TG-9 = 0.0 ± 0.1 km^3 yr^{-1}.
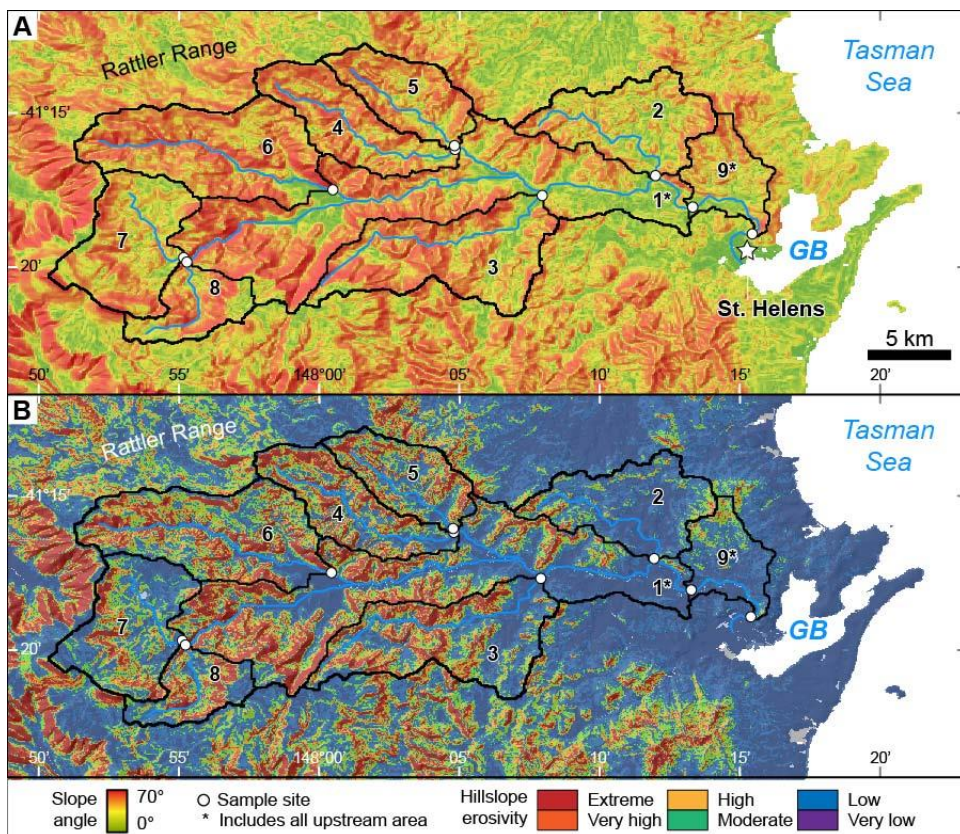
Figure 5: A. Map of hillslope angle across George River basin, derived from 90 m SRTM digital elevation models. B. Map of hillslope erosivity across George River basin, from Kidd et al. (2014, 2015). C. Analysis of variance, showing hillslope angles associated with categories of landscape erosivity (Kidd et al., 2014, 2015) at George River. Box-and-whiskers cover ±1.5x the interquartile range; black dot is the mean slope for the erosivity category. Comparison of means for each category indicate that the means of erosivity categories are all significantly different from each other (i.e. no categories are linked by the same letter in the Connecting Letters Report); we use hillslope angle as a quantitative proxy for erosivity at George River.

250
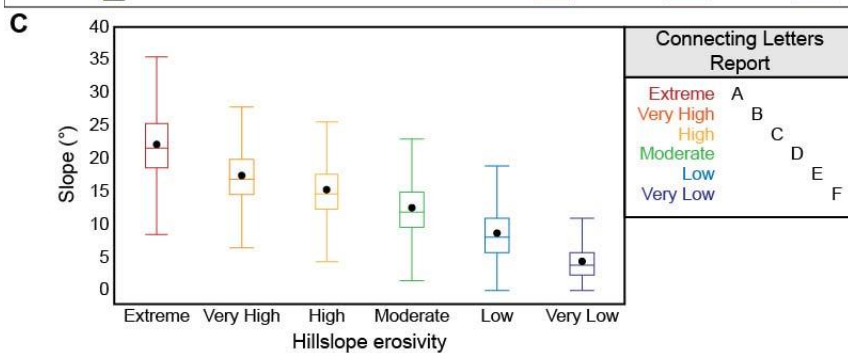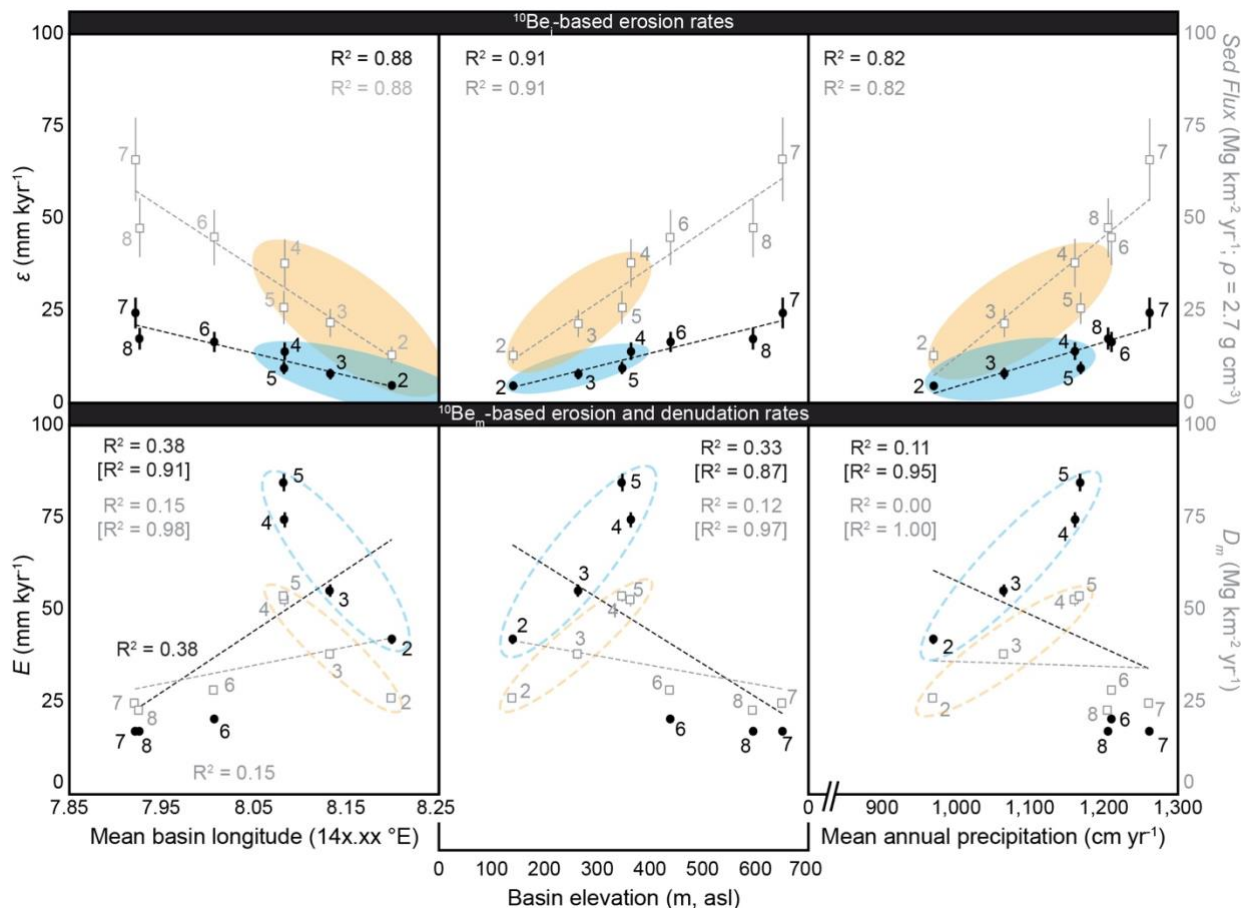
Figure 6: $^{10}Be_i$ based erosion rates (ε, top row, black circles), ε-based sediment fluxes (top row, gray squares), $^{10}Be_m$-based erosion rates (E, bottom row, black circles), and $^{10}Be_m/^9Be_{reac}$-based denudation rates (D_m, bottom row, gray squares) from George River tributaries compared to mean basin longitude, mean basin elevation, and mean annual precipitation within each basin. ε for all tributaries and E and D_m for the central and eastern tributaries (orange and blue ellipses, respectively) are strongly correlated with each variable, likely owing to the East-West precipitation gradient projected across the catchment (Fig. 3). Unbracketed R^2 values reflect correlation of all data whereas bracketed R^2 values indicate correlations for $^{10}Be_m$-based metrics only in the central and eastern tributaries. All error bars show 2σ uncertainties.
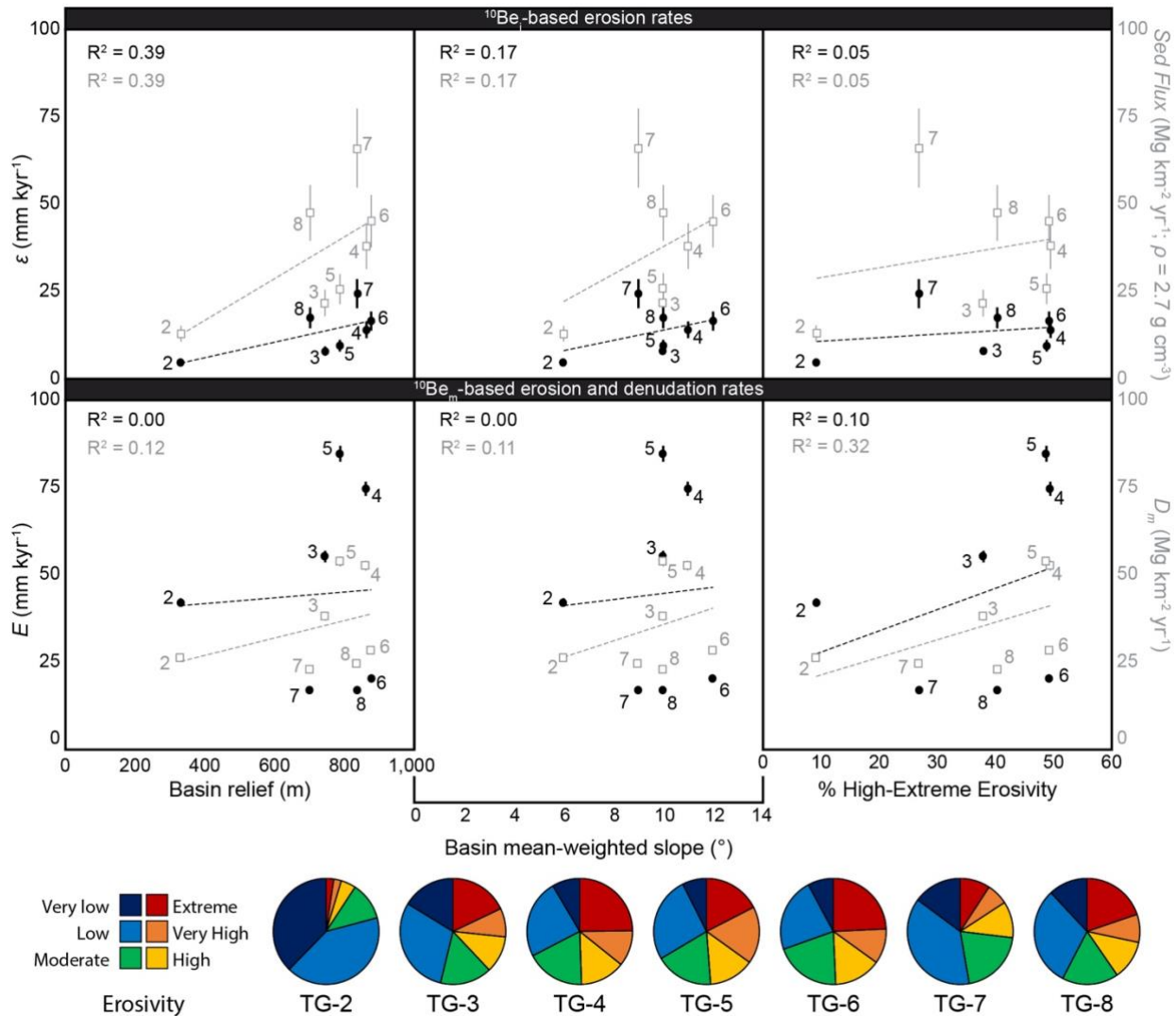
Figure 7: $^{10}Be_i$ based erosion rates (ε, top row, black circles), ε-based sediment fluxes (top row, gray squares), $^{10}Be_m$-based erosion rates (E, bottom row, black circles), and $^{10}Be_m/^9Be_{reac}$-based denudation rates (D_m, bottom row, gray squares) from George River tributaries compared to mean basin longitude, mean basin elevation, and mean annual precipitation within each basin. Moderate relationships exist between ε and basin relief and between D_m and the percent of each basin that is designated High Erosivity or greater (Kidd et al., 2014, 2015). All error bars show 2σ uncertainties.

4.2 $^{10}Be_m$ erosion rates, E, and denudation rates, D_m

$^{10}Be_m$-based erosion rates, E, range from 17.0 to 78.3 mm kyr^{-1} and replicate values for ε well in the three westernmost headwater catchments, but not in the lower-elevation, center and easternmost tributaries, where E is systematically ~5–6x higher than ε (Fig. 8). $^{10}Be_m/^9Be_{reac}$-based denudation rates, D_m, range from 22.7 to 53.7 Mg km^{-2} yr^{-1}. Except for TG-4 and TG-9, values for D_m do not replicate sediment fluxes derived from ε, although the central and easternmost tributaries plot much

closer to a 1:1 line than the samples from the three western-most headwater tributaries (Fig. 8). TG-4 was collected at the
285   mouth of Groom River, upstream of which activities at the long-closed Anchor Mine significantly altered the topography. The
meteoric erosion rate for the trunk channel site TG-9, $E = 78.3 \pm 2.2$ mm kyr^{-1} is significantly higher than ε for the same site
(10.7 ± 1.7 mm kyr^{-1}), but the denudation rate at TG-9, $D_m = 33.0 \pm 0.9$ Mg km^{-2} yr^{-1}, replicates the ε-based sediment flux (28.9 ± 4.5 Mg km^{-2} yr^{-1}).

290   In general, ^{10}Be$_m$-based measures of E and D_m are not significantly related to any topographic or climatic metric (Figs. 6, 7).
However, the observed relationships between E and D_m and longitude, elevation, and precipitation are similar to those observed
with ε in the central and eastern tributaries (Fig. 6); E and D_m in the western tributaries do not follow the spatial trends that ε
exhibits.
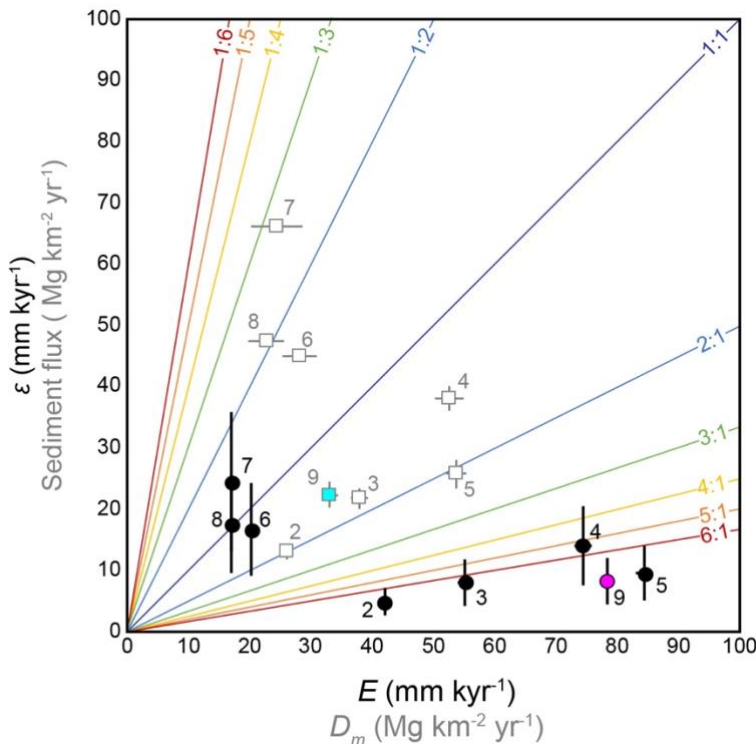
Figure 8: ^{10}Be$_i$-based erosion rates, ε, compared to ^{10}Be$_m$-based erosion rates, E (black circles) and ε-derived sediment fluxes compared to ^{10}Be$_m$/^{9}Be$_{reac}$-based denudation rates, D_m, (gray squares) for the same sample sites. Erosion rates for the trunk-channel sample, TG-9 are indicated by the magenta circle and denudation rates are indicated by the cyan square. All error bars show 2σ uncertainties. Solid colored lines indicate 1-fold through 6-fold differences between erosion and denudation metrics using the ^{10}Be$_i$ and ^{10}Be$_m$ methods. ^{10}Be$_m$ erosion rates are ~5–6x greater than ^{10}Be$_i$ erosion rates in the central and eastern tributaries. ^{10}Be$_m$/^{9}Be$_{reac}$ denudation rates replicate ^{10}Be$_i$ sediment fluxes with much greater accuracy than ^{10}Be$_m$ erosion rates.

295

5 Discussion

Erosion in George River is strongly related to basin longitude, elevation, and mean annual precipitation east of the Rattler
Range and the prominent Ben Lomond Plateau (Fig. 6), and we find no evidence to suggest that ε is related to slope in George
River over millennial timescales. This result differs from most studies, which show strong correlations between ε and mean
300   basin slope at a global scale (Portenga and Bierman, 2011), at regional scales, across the Great Dividing Range on Australia's
mainland (Fig. 9; Codilean et al., 2021; Nichols et al., 2014), and despite prior assessments of George River that suggest slope

imparts a large control over erosion and sediment generation in the catchment (Jerie et al., 2003; Kragt and Newham, 2009).

Instead, our finding is consistent with Mishra et al.'s (2018) suggestion that in low-slope, low-elevation, post-tectonic settings,

the relationship between slope and erosion becomes secondary to precipitation, and this study presents one of the clearest

305 examples of erosion along a topographically induced precipitation gradient in $^{10}Be_i$ erosion literature.
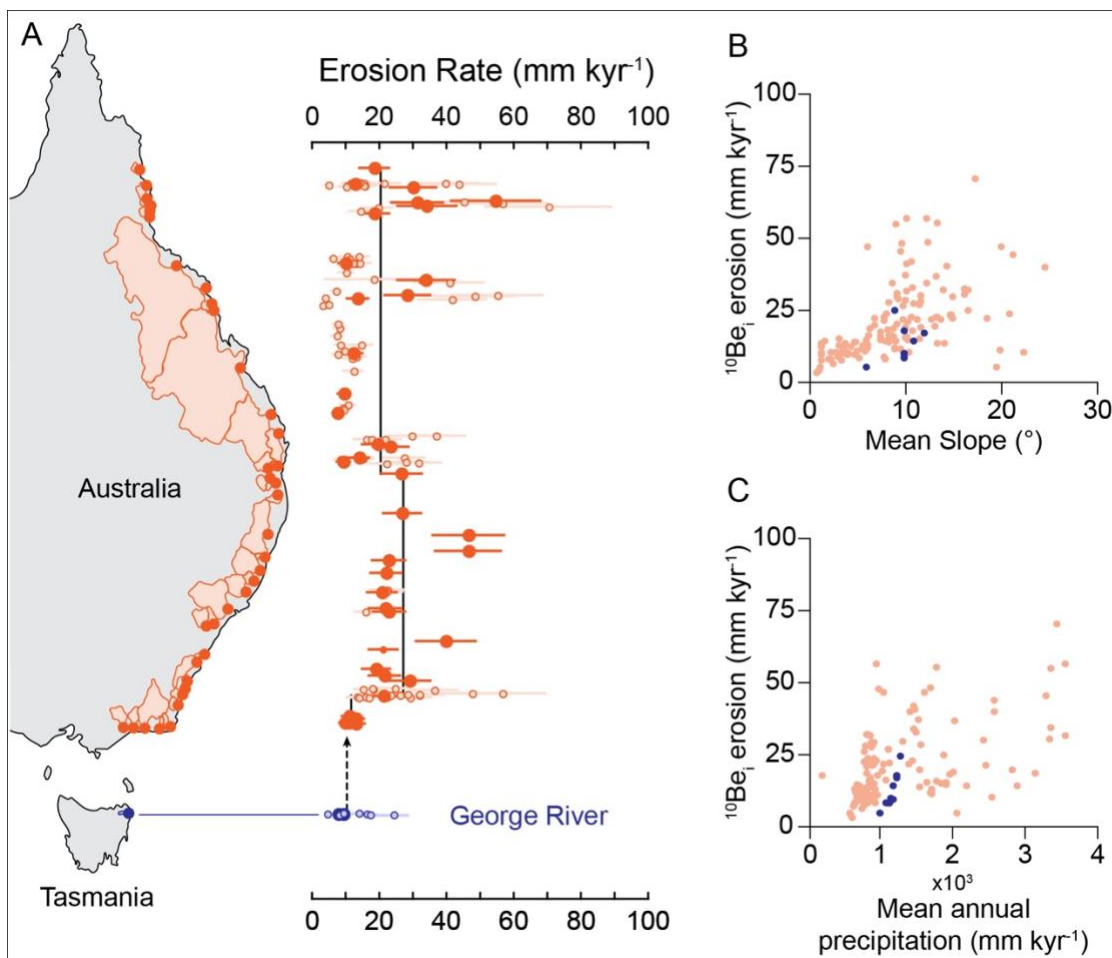
Figure 9: A. Map of river basins draining east off the Great Australian Escarpment, where $^{10}Be_i$ erosion rate data are available; adapted from Codilean et al. (2021). Filled circles are trunk streams and open circles are tributaries. Orange data include previously-published data (Codilean et al., 2021; Croke et al., 2015; Fülöp et al., 2020; Godard et al., 2019; Nichols et al., 2014; Tomkins et al.,
310 2007). Blue data are new data presented in this study from George River, Tasmania. The average $^{10}Be_i$ erosion rates from George River (10.5 mm kyr^{-1}) is consistent with erosion rates from southeast mainland Australia (average 11.6 mm kyr^{-1}; Codilean et al., 2021). **B.** Comparison of $^{10}Be_i$ erosion rates from George River (blue circles) and the eastern flanks of the Great Australian Escarpment (orange circles) to basin average slope. **B.** Comparison of $^{10}Be_i$ erosion rates from George River (blue circles) and the eastern flanks of the Great Australian Escarpment (orange circles) to mean annual precipitation.

315

The very strong relationship between precipitation and ε would likely not have emerged had our $^{10}Be_i$ samples been affected

by clast attrition (Carretier et al., 2009), deep-seated landslides (Aguilar et al., 2014; Gonzalez et al., 2016; Puchol et al., 2014),

or intensive erosion associated with mining, forestry, or agriculture (Barreto et al., 2014; Neilson et al., 2017). Even intensive

tin mining, which supplied >10^6 m^3 to George River over the last two centuries (Knighton, 1991) seems to not have not had a
320   long-lasting diluting effect on $^{10}Be_i$ in sampled stream sediment. It is possible that mining efforts, especially the sluice mining,
did not lead to $^{10}Be_i$ dilution because of the homogenizing effect of $^{10}Be_i$ in well-bioturbated soils (Brown et al., 1995) or that
the size of George River was large enough to buffer the effects of mining efforts in a similar way that large catchments can
buffer the effects of landslide material (Niemi et al., 2005; Yanites et al., 2009). It is also possible that mining activity did lead
to $^{10}Be_i$ dilution, but that these effects have since recovered along with bedload characteristics (Knighton, 1991) similar to the
325   rapid, two-year recovery of $^{10}Be_i$ concentrations following storm-triggered landslides in Puerto Rico (Grande et al., 2021).
Overall, the close relationship between $^{10}Be_i$ erosion rates and mean annual precipitation across George River demonstrates
how well $^{10}Be_i$ erosion rates can reflect background, geologically-meaningful rates of landscape evolution on millennial
timescales, even in areas with long histories of intensive human land-use.

330   Higher values of ε where there is more rainfall suggests that more sediment is being generated in the western portion of the
catchment where larger volumes of rainfall can facilitate the generation, erosion, entrainment, and delivery of sediment to
trunk channels than in the eastern portion of the catchment. However, we recognize that perhaps ε is not necessarily related to
precipitation, but rather ε and precipitation may both be more directly influenced by elevation. Although no part of George
River was ever glaciated, cirque development and periglacial activity was active to the southwest of George River, across the
335   Ben Lomond Plateau during the Last Glacial Maximum and previous glaciations (Barrows et al., 2002; Colhoun, 2002), in
which case ε may be greater at higher elevations due to greater amounts of periglacial weathering.

High $^{10}Be_i$ erosion rates have been linked to greater amounts of periglacial activity elsewhere (e.g. Delunel et al., 2010;
Hancock and Kirwan, 2007; Marshall et al., 2017); however, periglacial activity in northeast Tasmania was typically limited
340   to elevations >1,100 m (Colhoun, 2002), and it is therefore unlikely that periglacial processes would have increased erosion
rates in George River's western tributaries, all of which are below this elevation. Alternatively, higher ε at higher elevations
may be due to greater amounts of rock exhumation for inland northeast Tasmania relative to the coasts throughout the
Cenozoic, interpolated from apatite fission track cooling ages across Tasmania (Kohn et al., 2002). This is also unlikely,
however, as landscape lowering over millions of years has slowed from an early Cenozoic peak rates of 30–50 m Myr^{-1} to late
345   Cenozoic rates of <10 m Myr^{-1}, and rock exhumation rates are presently comparable, if not slower than new $^{10}Be_i$ based erosion
rates presented in this study. We therefore remain confident that the relationship between ε and elevation and rainfall in this
study are real and reflective of the influence of rainfall in driving landscape evolution over millennial timescales in George
River.

350   Since pre-disturbance stream flow and bedload conditions were re-established by the 1990s (Knighton, 1991), it appears the
greatest risk of future excesses of sediment flux from George River to Georges Bay comes from land-use changes involving
the widespread disturbance of surficial soils, such as through forestry (Wilson, 1999). The percentage of land used for

Production forestry in native environments has been decreasing throughout the 21st century (Fig. 4), and while some of this land use is being supplanted by Conservation and Protected Native Land Cover, which could buffer the effects of widespread

355   erosion, much is being replaced by grazing and agriculture, which would only serve to increase erosion, particularly in the headwater catchments where geological erosion rates are naturally high (Fig. 4). Given recent land-use trends, the ^{10}Be$_i$ erosion rates presented here may provide a useful benchmark level of sediment delivery to George River, Georges Bay, and other fluvial systems in northeast Tasmania that share topographic and geologic characteristics similar to those at George River.

360   **5.1 Considerations of ε for trunk channel versus tributary sites**

A mass-balance comparison of the volume of sediment passing through the trunk channels (ε x upstream area; 3.8 ± 0.7 km^3 yr^{-1} at TG-1 and 3.5 ± 0.7 km^3 yr^{-1} at TG-9) versus the summed volume of sediment exiting tributaries (3.9 ± 0.3 km^3 yr^{-1}) suggests that little erosion (and therefore addition of sediment) is occurring in the trunk channel subcatchments. Average modelled ε for trunk channel sites, calculated using the regression equations and mean longitude, the mean elevation, and mean

365   annual precipitation values for the TG-1 and TG-9 subcatchments (9.6 ± 3.0 mm kyr^{-1} and 1.1 ± 3.1 mm kyr^{-1}, respectively), however, suggests that the TG-1 subcatchment should be contributing at least ~1 km^3 of sediment more to George River annually. Given that the mass of sediment leaving the tributaries is equal to the mass of sediment passing through TG-1 and TG-9, we make the interpretation that the ^{10}Be$_i$ measured at TG-1 and TG-9 trunk channel locations is effectively dominated by erosion in the tributaries, with little input from the subcatchments or George River floodplain, and ε at trunk channel sites

370   should be considered minimum estimates of erosion for the upstream contributing area. Our interpretation of erosion at trunk streams being dominated by headwater input has been made elsewhere, albeit in much larger river basins (i.e. Wittmann et al. 2009, 2011, 2016). The average erosion rate we therefore present for George River is the average of ε at TG-1, TG-9, and the average of ε from the seven tributaries combined (10.5 ± 0.8 mm kyr^{-1}); we do not consider ε of trunk channel samples, modelled or measured, when considering spatial statistics of erosion in George River basin.

375

Compared to measurements of ε on the Australian mainland, the mean value of ε for George River (10.5 ± 0.8 mm kyr^{-1}) is of similar magnitude as the median erosion rate for all catchments draining the eastern flanks of the Great Dividing Range passive margin of mainland Australia (15.9 mm kyr^{-1}; Fig. 9; Codilean et al., 2021). Average ε from George River is most consistent, however, with the erosion rates of mainland basins at the southernmost extent of the Great Dividing Range, across the Bass

380   Strait, which are those that share similar topographic characteristics and geological histories as George River (Codilean et al., 2021). The similarity between the geology, climate, and topography of newly-sampled basins and derived ^{10}Be$_i$ erosion rates in Tasmania and those from southeast mainland Australia suggests that evolution of landscapes that share similar climatic, topographic, and geologic characteristics is driven by common forces.

385

5.2 Comparing $^{10}Be_i$-based and $^{10}Be_m$-based erosion and denudation metrics

The strong relationship between $^{10}Be_i$ erosion rates and topographically-induced precipitation across Georges River (Fig. 6) suggests that $^{10}Be_i$ erosion rates, ε, are geologically accurate and meaningful. The small, geologically-homogeneous landscape

390   of George River, therefore allows us to test a previous hypothesis (Portenga et al., 2019) that measured $^{10}Be_m$-based erosion rates, E, and $^{10}Be_m/^9Be_{reac}$-based denudation rates, D_m, to replicate ε or ε-based sediment fluxes, respectively. At first glance, E replicates ε only in the headwater catchments and D_m replicates ε-based sediment fluxes relatively well in all tributaries except for the headwater catchments (Fig. 8). Overall, values of E and D_m do not replicate the spatial patterns or yield the same relationships with topographic and climate parameters that we observe with ε and ε-based sediment fluxes (Figs. 6, 7).

395   However, when only E and D_m from tributaries in the central and eastern areas of George River (TG-2 through TG-5) are considered, a consistent relationship between E and D_m and basin longitude, elevation, and precipitation emerges and is similar to the relationships we observe between longitude, elevation, and precipitation and ε (Fig. 6). Despite this small sample subset ($n = 4$), we suggest that E and D_m reflect the same patterns of landscape dynamics in George River as ε. Moreover, the similarity of D_m and ε-based sediment fluxes for central and eastern tributaries provides support our hypothesis that $^{10}Be_m/^9Be_{reac}$ based

400   denudation rates should more-closely replicate $^{10}Be_i$-based erosion rates in small river basins where geological heterogeneity is minimized. Our findings also, generally, support the continued exploration and application of $^{10}Be_m/^9Be_{reac}$ denudation rates in geomorphological studies (Dannhaus et al., 2017; Deng et al., 2020; Portenga et al., 2019; Rahaman et al., 2017; Wittmann et al., 2012, 2015). Interestingly, measured values of E are systematically ~4–5x greater than ε, and thus while E may be influenced by the same geomorphological processes in George River as ε and D_m, it does not appear to reflect accurate rates

405   of landscape change.

The similarity of the spatial patterns of E and D_m with longitude, elevation, and precipitation in the central and eastern tributaries with those exhibited by ε across the whole George River basin suggests that E and D_m in the headwater catchments (TG-6, TG-7, and TG-8) significantly underestimate accurate or realistic values of E and D_m for these tributaries. Of all of the

410   variables and measurements required to derive both E and D_m, excess amounts of measured $^{10}Be_m$ is the only common factor that would lead to erroneously low calculated values of E and D_m. Once delivered to Earth's surface, meteoric $^{10}Be_m$ concentrates in uppermost soil horizons (Graly et al., 2010; Willenbring and von Blanckenburg, 2010), and thus any disturbance and excavation of large volumes of topsoil (i.e. agriculture, forestry, wildfire erosion, or mining activities) could strip soil with the highest concentrations of $^{10}Be_m$ in its grain coatings entering and introduce them into a stream's bedload, a

415   process similar to that identified following early land-use changes and deforestation in the Chesapeake Bay and San Francisco Bay (Valette-Silver et al., 1986; van Geen et al., 1999). Mining activities in George River were restricted to lower catchment areas and tributaries where $^{10}Be_m$ based metrics demonstrate the same relationships to topography and climate as ε (Fig. 2), and no wildfires nor prescribed fires have burned through the headwater catchments (Fig. 4).

420   At the time of sample collection for this study in 2008, forestry from natural environments and from production plantations was the largest land use designation within George River. Elsewhere in George River, rainfall and runoff experiments carried out in the Gentle Annie experimental catchment, a tributary to TG-2 (Fig. 4), showed that rills and gullies developed in hillslope plots that were heavily disturbed by forestry machinery, yielding significantly more sediment during simulated rainfall events than soil plots that were burned and more sediment than plots where soils were left undisturbed (Wilson, 1999). Although

425   there are no detailed records of when plots of land in George River were timbered, we invoke Wilson's (1999) findings to suggest it is plausible that active forestry had disturbed soils in the headwater catchments at or shortly prior to the timing of sample collection, significantly disturbing $^{10}Be_m$-rich top soils, and delivering large volumes of sediment with excess $^{10}Be_m$ to sample collection sites, which subsequently resulted in the calculated values of E and D_m that are much lower than otherwise expected based on the trends of E and D_m in other tributaries. Following this interpretation, we suggest that measures of E and

430   D_m may reflect spatial patterns or replicate ε rates in geologically homogeneous landscapes, respectively, but caution should be taken when applying $^{10}Be_m$ erosion and denudation metrics in landscapes with intensive soil disturbances (Portenga et al., 2019).

6 Conclusions

435   $^{10}Be_i$ erosion rates throughout the George River basin, and $^{10}Be_m$ erosion and denudation rates in its central and eastern tributaries, are closely related to a topographically-induced East-West precipitation gradient across the catchment. Tasmanian landscapes differ from the Great Dividing Range where erosion rates and slope are closely linked. The average $^{10}Be_i$ erosion in George River, 13.6 mm kyr^{-1}, reflects erosion in tributaries to George River where precipitation is greatest; little sediment is generated in trunk channel subcatchments. These findings support the notion that precipitation imparts more influence on

440   landscape development in low-slope, low-elevation landscapes (Mishra et al., 2018), which often tend to be in post-orogenic, passive margin settings.

Although sediment erosion associated with mining, agricultural, and forestry land-use practices occurred in the George River basin during the 19th and 20th Centuries, $^{10}Be_i$ based erosion rates in the basin appear to reflect pre-disturbance rates of

445   landscape change. Such rates are useful as part of Tasmania's current efforts to re-establish healthy and sustainable ecological conditions in its many estuarine environments, particularly those in northeast Tasmania where estuary tributaries have similar geological and topographic characteristics to those found at George River. The pace of erosion in the George River basin is similar to that at the southern end of the Great Dividing Range on the Australian mainland, which has similar bedrock and climate characteristics.

450

$^{10}Be_m$-based erosion and denudation in the central and eastern tributaries of George River generally replicates spatial patterns of $^{10}Be_i$-based erosion and denudation. Low $^{10}Be_m$-based erosion and denudation rates calculated in three headwater tributaries demonstrate the sensitivity of meteoric ^{10}Be-based calculation to recent and intensive land use that disturbs and erodes topsoils.

Data from the George River basin support application of $^{10}Be_m$ methods in small, lithologically homogeneous basins with

455   limited amounts of topsoil disturbance.

Appendices

Appendix A: Erosion rate and denudation rate equations

$^{10}Be_i$ Erosion Rate

$$\varepsilon = \frac{\Lambda \left(\frac{P_0}{N} - \lambda\right)}{\rho}$$

$^{10}Be_i$ Sediment Flux

$$Sed\ Flux = \varepsilon\,\rho$$

$^{10}Be_i$ Integration Time

$$Int\ Time = \frac{\Lambda\,\varepsilon}{\rho}$$

$^{10}Be_m$ Erosion Rate [d]

$$E = \frac{Q}{\rho\ ^{10}Be_m}$$

$^{10}Be_m/^9Be_{reac}$ Denudation Rate [e]

$$D_m = \frac{Q\left(\frac{^9Be_{min}}{^9Be_{reac}} + 1\right)}{\left(\frac{^{10}Be_m}{^9Be_{reac}}\right)\ ^9Be_{parent}}$$

Variable	Description	Unit
ϵ	$^{10}Be_i$ erosion rate	cm yr^{-1}
Λ	Attenuation length for cosmic-ray penetration[a]	160 g cm^{-2}
P_0	Production rate of $^{10}Be_i$ at Earth's surface[b]	atoms g^{-1} yr^{-1}
N	Measured concentration of in-situ produced $^{10}Be_i$	atoms g^{-1}
λ	^{10}Be decay constant[c]	yr^{-1}
ρ	Rock density	2.7 g cm^{-3}
E	$^{10}Be_m$-based erosion rate	cm yr^{-1}
Q	Atmospheric $^{10}Be_m$ delivery rate	atoms cm^{-2} yr^{-1}
$^{10}Be_m$	Measured concentration of $^{10}Be_m$ extracted from sediment grain coatings	atoms g^{-1}
D_m	$^{10}Be_m/^9Be_{reac}$-based denudation rate	g cm^{-2} yr^{-1}
$^9Be_{min}$	Measured concentration of ^9Be still within mineral grains	atoms g^{-1}
$^9Be_{reac}$	Measured concentration of ^9Be extracted from sediment grain coatings	atoms g^{-1}
$^9Be_{parent}$	Assumed concentration of ^9Be in crustal bedrock[f]	1.671 x 10^{17} atoms g^{-1}

[a] Balco et al. (2008), Gosse and Phillips (2001)
[b] Scaled for each basin following Lal (1991) and Stone (2000)
[c] Half-life of ^{10}Be = 1.36 Myr
[d] Willenbring and von Blanckenburg (2010)
[e] von Blanckenburg et al. (2012)
[f] Derived from an assumed value of 2.55 ppm, following von Blanckenburg et al. (2012)

Appendix B: CRONUS Entry Data

TG-1	-41.29017	148.22217	346	std	1	2.7	0	2008	;	
TG-1	Be-10	Quartz	3.64E+05	6.52E+03	07KNSTD	;				
TG-2	-41.27183	148.19925	141	std	1	2.7	0	2008	;	
TG-2	Be-10	Quartz	5.66E+05	7.72E+03	07KNSTD	;				
TG-3	-41.28286	148.13247	265	std	1	2.7	0	2008	;	
TG-3	Be-10	Quartz	3.97E+05	1.17E+04	07KNSTD	;				
TG-4	-41.25514	148.08317	364	std	1	2.7	0	2008	;	
TG-4	Be-10	Quartz	2.56E+05	6.95E+03	07KNSTD	;				
TG-5	-41.25364	148.08239	347	std	1	2.7	0	2008	;	
TG-5	Be-10	Quartz	3.63E+05	8.48E+03	07KNSTD	;				
TG-6	-41.28067	148.00697	439	std	1	2.7	0	2008	;	
TG-6	Be-10	Quartz	2.33E+05	5.05E+03	07KNSTD	;				
TG-7	-41.32208	147.92172	652	std	1	2.7	0	2008	;	
TG-7	Be-10	Quartz	1.88E+05	5.60E+03	07KNSTD	;				
TG-8	-41.32178	147.92592	596	std	1	2.7	0	2008	;	
TG-8	Be-10	Quartz	2.48E+05	6.10E+03	07KNSTD	;				
TG-9	-41.31350	148.26531	331	std	1	2.7	0	2008	;	
TG-9	Be-10	Quartz	4.11E+05	9.92E+03	07KNSTD	;				

460

Data Availability

All data used in this study, and all data needed to reproduce our findings are presented in Tables 1-3 and the equations we use to work with data to calculate erosion rates, sediment fluxes, denudation rates, and integration times are presented in Appendix

465   A. Data entry for calculating erosion rates from the CRONUS online erosion rate calculator, formatted for text entry, are given in Appendix.

Author Contribution

The conceptual analysis of the data presented in this paper comes from LV's Undergraduate Honors Thesis (2020) at Eastern

470   Michigan University. EWP contributed to post-thesis manuscript revisions, data analysis, and figure drafting. Samples and the $^{10}Be_i$ data presented here were collected and facilitated by PRB and ECL in 2008. ^{9}Be and $^{10}Be_m$ data were first presented in Sophie E. Greene's Master's Thesis (2016) at the University of Vermont; SEG declined a request to participate in the writing and publication of this paper. AJH verified Lawrence Livermore National Laboratory's measurement of beryllium at the Center for Accelerator Mass Spectrometry in 2009. This work was performed in part under the auspices of the U.S. Department of

475   Energy by Lawrence Livermore National Laboratory under Contract DE-AC52- 07NA27344. This is LLNL-JRNL-825534.

References

ABARES, 2016, The Australian Land Use and Management Classification Version 8: Australian Bureau of Agricultural and Resource Economics and Sciences, https://www.agriculture.gov.au/abares/aclump/land-use/alum-classification.

480   Adams, B. A., and Ehlers, T., 2017, Deciphering topographic signals of glaciation and rock uplift in an active orogen: A case study from the Olympic Mountains, USA: Earth Surface Processes and Landforms, v. 42, no. 11, p. 1680-1692.

Aguilar, G., Carretier, S., Regard, V., Vassallo, R., Riquelme, R., and Martinod, J., 2014, Grain size-dependent 10Be concentrations in alluvial stream sediment of the Huasco Valley, a semi-arid Andes region: Quaternary Geochronology, v. 19, p. 163-172.

485   Augustinus, P., Barton, C. E., Zawadzki, A., and Harle, K., 2010, Lithological and geochemical record of mining-induced changes in sediments from Macquarie Harbour, southwest Tasmania, Australia: Environmental Earth Sciences, v. 61, no. 3, p. 625-639.

Balco, G., Stone, J. O., Lifton, N. A., and Dunai, T. J., 2008, A complete and easily accessible means of calculating surface exposure ages or erosion rates from 10Be and 26Al measurements: Quaternary Geochronology, v. 3, no. 3, p. 174-195.

490   Barreto, H. N., Varajão, C. A. C., Braucher, R., Bourlès, D. L., Salgado, A. A. R., and Varajão, A. F. D. C., 2014, The impact of diamond extraction on natural denudation rates in the Diamantina Plateau (Minas Gerais, Brazil): Journal of South American Earth Sciences, v. 56, p. 357-364.

Barrows, T. T., Stone, J. O., Fifield, L. K., and Cresswell, R. G., 2001, Late Pleistocene Glaciation of the Kosciuszko Massif, Snowy Mountains, Australia: Quaternary Research, v. 55, no. 2, p. 179-189.

495   -, 2002, The timing of the Last Glacial Maximum in Australia: Quaternary Science Reviews, v. 21, no. 1, p. 159-173.

Batley, G., Crawford, C., Moore, M., McNeil, J., Reid, J., Koehnken, L., and Ramsay, J., 2010, Report of the George River Water Quality Panel.

Beard, J., Crawford, C., and Hirst, A., 2008, Developing a Monitoring Program for Six Key Estuaries in North-west Tasmania: Tasmanian Aquaculture and Fisheries Institute.

500   Belmont, P., Pazzaglia, F., and Gosse, J. C., 2007, Cosmogenic 10Be as a tracer for hillslope and channel sediment dynamics in the Clearwater River, western Washington State: Earth and Planetary Science Letters, v. 264, no. 1-2, p. 123-135.

Bierman, P., and Steig, E. J., 1996, Estimating rates of denudation using cosmogenic isotope abundances in sediment: Earth surface processes and landforms, v. 21, no. 2, p. 125-139.

Bleaney, A., Hickey, C. W., Stewart, M., Scammell, M., and Senjen, R., 2015, Preliminary investigations of toxicity in the Georges Bay catchment, Tasmania, Australia: International Journal of Environmental Studies, v. 72, no. 1, p. 1-23.

BoM, 2021, Climate Data Online: Australia Bureau of Meteorology, http://www.bom.gov.au/climate/data/.

Braucher, R., Brown, E., Bourlès, D., and Colin, F., 2003, In situ produced 10Be measurements at great depths: implications for production rates by fast muons: Earth and Planetary Science Letters, v. 211, no. 3-4, p. 251-258.

Brown, E. T., Stallard, R. F., Larsen, M. C., Raisbeck, G. M., and Yiou, F., 1995, Denudation rates determined from the accumulation of in situ-produced 10Be in the Luquillo Experimental Forest, Puerto Rico: Earth and Planetary Science Letters, v. 129, no. 1-4, p. 193-202.

Brown, L., Pavich, M. J., Hickman, R. E., Klein, J., and Middleton, R., 1988, Erosion of the eastern United States observed with 10Be: Earth Surface Processes and Landforms, v. 13, no. 5, p. 441-457.

Butler, E. C., 2006, The tail of two rivers in Tasmania: the Derwent and Huon estuaries, Estuaries, Springer, p. 1-49.

Carretier, S., Regard, V., and Soual, C., 2009, Theoretical cosmogenic nuclide concentration in river bed load clasts: Does it depend on clast size?: Quaternary Geochronology, v. 4, no. 2, p. 108-123.

Carretier, S., Tolorza, V., Regard, V., Aguilar, G., Bermúdez, M. A., Martinod, J., Guyot, J. L., Hérail, G., and Riquelme, R., 2018, Review of erosion dynamics along the major NS climatic gradient in Chile and perspectives: Geomorphology, v. 300, p. 45-68.

Carretier, S., Tolorza, V., Rodríguez, M., Pepin, E., Aguilar, G., Regard, V., Martinod, J., Riquelme, R., Bonnet, S., and Brichau, S., 2015, Erosion in the Chilean Andes between 27 S and 39 S: tectonic, climatic and geomorphic control: Geological Society, London, Special Publications, v. 399, no. 1, p. 401-418.

Cheetham, M. D., and Martin, J. C., 2018, Hope for the best, plan for the worst: Managing sediment input in the upper catchment whilst preparing for avulsion at the mouth, 9th Australian Stream Management Conference: Hobart, Tasmania, Australia, p. 8.

Codilean, A. T., Fülöp, R.-H., Munack, H., Wilcken, K. M., Cohen, T. J., Rood, D. H., Fink, D., Bartley, R., Croke, J., and Fifield, L., 2021, Controls on denudation along the East Australian continental margin: Earth-Science Reviews, p. 103543.

Codilean, A. T., Munack, H., Cohen, T. J., Saktura, W. M., Gray, A., and Mudd, S. M., 2018, OCTOPUS: an open cosmogenic isotope and luminescence database: Earth System Science Data, v. 10, no. 4, p. 2123-2139.

Colhoun, E. A., 2002, Periglacial landforms and deposits of Tasmania : Periglacial and Permafrost Research in the Southern Hemisphere: South African Journal of Science, v. 98, no. 1, p. 55-63.

Corbett, L. B., Bierman, P. R., and Rood, D. H., 2016, An approach for optimizing in situ cosmogenic 10Be sample preparation: Quaternary Geochronology, v. 33, p. 24-34.

Cosgrove, R., 1995, Late Pleistocene behavioural variation and time trends: the case from Tasmania: Archaeology in Oceania, v. 30, no. 3, p. 83-104.

Cosgrove, R., Allen, J., and Marshall, B., 1990, Palaeo-ecology and Pleistocene human occupation in south central Tasmania: Antiquity, v. 64, no. 242, p. 59-78.

Coughanowr, C., and Whitehead, J., 2013, The Derwent Estuary Program: A collaborative model for science-based management, Tasmania, Australia: Ocean & Coastal Management, v. 86, p. 110-118.

Crawford, C., and White, C., 2005, Establishment of an integrated water quality monitoring framework for Georges Bay.

Creighton, C., Boon, P. I., Brookes, J. D., and Sheaves, M., 2015, Repairing Australia's estuaries for improved fisheries production – what benefits, at what cost?: Marine and Freshwater Research, v. 66, no. 6, p. 493-507.

Croke, J., Bartley, R., Chappell, J., Austin, J. M., Fifield, K., Tims, S. G., Thompson, C. J., and Furuichi, T., 2015, 10Be-derived denudation rates from the Burdekin catchment: The largest contributor of sediment to the Great Barrier Reef: Geomorphology, v. 241, p. 122-134.

Crowder, E., Rawlinson, N., Pilia, S., Cornwell, D. G., and Reading, A. M., 2019, Transdimensional ambient noise tomography of Bass Strait, southeast Australia, reveals the sedimentary basin and deep crustal structure beneath a failed continental rift: Geophysical Journal International, v. 217, no. 2, p. 970-987.

Dannhaus, N., Wittmann, H., Krám, P., Christl, M., and von Blanckenburg, F., 2018, Catchment-wide weathering and erosion rates of mafic, ultramafic, and granitic rock from cosmogenic meteoric 10Be/9Be ratios: Geochimica et Cosmochimica Acta, v. 222, p. 618-641.

Davis, J., and Kidd, I. M., 2012, Identifying Major Stressors: The Essential Precursor to Restoring Cultural Ecosystem Services in a Degraded Estuary: Estuaries and Coasts, v. 35, no. 4, p. 1007-1017.

Delunel, R., Schlunegger, F., Valla, P. G., Dixon, J., Glotzbach, C., Hippe, K., Kober, F., Molliex, S., Norton, K. P., Salcher, B., Wittmann, H., Akçar, N., and Christl, M., 2020, Late-Pleistocene catchment-wide denudation patterns across the European Alps: Earth-Science Reviews, v. 211, p. 103407.

Delunel, R., van der Beek, P. A., Carcaillet, J., Bourlès, D. L., and Valla, P. G., 2010, Frost-cracking control on catchment denudation rates: Insights from in situ produced 10Be concentrations in stream sediments (Ecrins–Pelvoux massif, French Western Alps): Earth and Planetary Science Letters, v. 293, no. 1-2, p. 72-83.

Deng, K., Yang, S., von Blanckenburg, F., and Wittmann, H., 2020, Denudation Rate Changes Along a Fast-Eroding Mountainous River With Slate Headwaters in Taiwan From 10Be (Meteoric)/9Be Ratios: Journal of Geophysical Research: Earth Surface, v. 125, no. 2, p. e2019JF005251.

Dethier, D. P., Ouimet, W., Bierman, P. R., Rood, D. H., and Balco, G., 2014, Basins and bedrock: Spatial variation in 10Be erosion rates and increasing relief in the southern Rocky Mountains, USA: Geology, v. 42, no. 2, p. 167-170.

Edgar, G., and Barrett, N., 2000, Effects of Catchment Activities on Macrofaunal Assemblages in Tasmanian Estuaries: Estuarine, Coastal and Shelf Science, v. 50, no. 5, p. 639-654.

Edgar, G. J., Barrett, N. S., Graddon, D. J., and Last, P. R., 2000, The conservation significance of estuaries: a classification of Tasmanian estuaries using ecological, physical and demographic attributes as a case study: Biological Conservation, v. 92, no. 3, p. 383-397.

Elliott, M., Burdon, D., Hemingway, K. L., and Apitz, S. E., 2007, Estuarine, coastal and marine ecosystem restoration: confusing management and science–a revision of concepts: Estuarine, Coastal and Shelf Science, v. 74, no. 3, p. 349-366.

Ellison, J. C., and Sheehan, M. R., 2014, Past, present and futures of the Tamar Estuary, Tasmania, Estuaries of Australia in 2050 and Beyond, Springer, p. 69-89.

Etheridge, M. A., Branson, J. C., and Stuart-Smith, P. G., 1987, The Bass, Gippsland and Otway basins, southeast Australia: A branched rift system formed by continental extension: Sedimentary Basins and Basin-forming Mechanisms, v. Memoir 12, p. 147-162.

Fellin, M. G., Chen, C.-Y., Willett, S. D., Christl, M., and Chen, Y.-G., 2017, Erosion rates across space and timescales from a multi-proxy study of rivers of eastern Taiwan: Global and Planetary Change, v. 157, p. 174-193.

Ferrier, K. L., Kirchner, J. W., and Finkel, R. C., 2005, Erosion rates over millennial and decadal timescales at Caspar Creek and Redwood Creek, northern California Coast Ranges: Earth Surface Processes and Landforms: The Journal of the British Geomorphological Research Group, v. 30, no. 8, p. 1025-1038.

Fick, S. E., and Hijmans, R. J., 2017, WorldClim 2: new 1-km spatial resolution climate surfaces for global land areas: International Journal of Climatology, v. 37, no. 12, p. 4302-4315.

Fitzsimons, J. A., Hale, L., Hancock, B., and Beck, M. W., 2015, Developing a marine conservation program in temperate Australia: determining priorities for action: Australian Journal of Maritime & Ocean Affairs, v. 7, no. 1, p. 85-93.

Foster, D. A., and Gray, D. R., 2000, Evolution and Structure of the Lachlan Fold Belt (Orogen) of Eastern Australia: Annual Review of Earth and Planetary Sciences, v. 28, no. 1, p. 47-80.

Fülöp, R.-H., Codilean, A. T., Wilcken, K. M., Cohen, T. J., Fink, D., Smith, A. M., Yang, B., Levchenko, V. A., Wacker, L., Marx, S. K., Stromsoe, N., Fujioka, T., and Dunai, T. J., 2020, Million-year lag times in a post-orogenic sediment conveyor: Science Advances, v. 6, no. 25, p. eaaz8845.

Gaina, C., Müller, D. R., Royer, J.-Y., Stock, J., Hardebeck, J., and Symonds, P., 1998, The tectonic history of the Tasman Sea: A puzzle with 13 pieces: Journal of Geophysical Research: Solid Earth, v. 103, no. B6, p. 12413-12433.

Gallant, J., Wilson, N., Dowling, T., Read, A., and Inskeep, C., 2011, SRTM-derived 1 Second Digital Elevation Models Version 1.0. Record 1: Geoscience Australia, Canberra, ACT, Australia.

Gee, R. D., and Groves, D. I., 1971, Structural features and mode of emplacement of part of the blue tier batholith in Northeast Tasmania: Journal of the Geological Society of Australia, v. 18, no. 1, p. 41-55.

Geist, J., and Hawkins, S. J., 2016, Habitat recovery and restoration in aquatic ecosystems: current progress and future challenges: Aquatic Conservation: Marine and Freshwater Ecosystems, v. 26, no. 5, p. 942-962.

Godard, V., Dosseto, A., Fleury, J., Bellier, O., and Siame, L., 2019, Transient landscape dynamics across the Southeastern Australian Escarpment: Earth and Planetary Science Letters, v. 506, p. 397-406.

Gonzalez, V. S., Bierman, P. R., Nichols, K. K., and Rood, D. H., 2016, Long-term erosion rates of Panamanian drainage basins determined using in situ 10Be: Geomorphology, v. 275, p. 1-15.

Gosse, J. C., and Phillips, F. M., 2001, Terrestrial in situ cosmogenic nuclides: theory and application: Quaternary Science Reviews, v. 20, no. 14, p. 1475-1560.

605   Graly, J. A., Bierman, P. R., Reusser, L. J., and Pavich, M. J., 2010, Meteoric 10Be in soil profiles – A global meta-analysis: Geochimica et Cosmochimica Acta, v. 74, no. 23, p. 6814-6829.

Graly, J. A., Reusser, L. J., and Bierman, P. R., 2011, Short and long-term delivery rates of meteoric 10Be to terrestrial soils: Earth and Planetary Science Letters, v. 302, no. 3, p. 329-336.

Grande, A., Schmidt, A. H., Bierman, P. R., Corbett, L. B., López-Lloreda, C., Willenbring, J., McDowell, W. H., and Caffee, 610   M. W., 2021, Landslides, hurricanes, and sediment sourcing impact basin-scale erosion estimates in Luquillo, Puerto Rico: Earth and Planetary Science Letters, v. 562, p. 116821.

Granger, D. E., Kirchner, J. W., and Finkel, R., 1996, Spatially averaged long-term erosion rates measured from in situ-produced cosmogenic nuclides in alluvial sediment: The Journal of Geology, v. 104, no. 3, p. 249-257.

Gray, D. R., and Foster, D. A., 2004, Tectonic evolution of the Lachlan Orogen, southeast Australia: Historical review, data 615   synthesis and modern perspectives: Australian Journal of Earth Sciences, v. 51, no. 6, p. 773-817.

Greene, E. S., 2016, Comparing meteoric 10Be, in situ 10Be, and native 9Be across a diverse set of watersheds, Master's Thesis, Geology Department, University of Vermont, Burlington, VT, United States, 118 p.

Griffiths, J. R., 1971, Continental margin tectonics and the evolution of south-east Australia: The APPEA Journal, v. 11, no. 1, p. 75-79.

620   Gunn, P. J., 1975, Mesozoic-Cainozoic Tectonics and Igneous Activity: Southeastern Australia: Journal of the Geological Society of Australia, v. 22, no. 2, p. 215-221.

Hancock, G., and Kirwan, M., 2007, Summit erosion rates deduced from 10Be: Implications for relief production in the central Appalachians: Geology, v. 35, no. 1, p. 89-92.

Harel, M.-A., Mudd, S., and Attal, M., 2016, Global analysis of the stream power law parameters based on worldwide 10Be 625   denudation rates: Geomorphology, v. 268, p. 184-196.

Harrison, E. J., Willenbring, J. K., and Brocard, G. Y., 2021, Quaternary record of terrestrial environmental change in response to climatic forcing and anthropogenic perturbations, in Puerto Rico: Quaternary Science Reviews, v. 253, p. 106770.

Hayes, D. E., and Ringis, J., 1973, Seafloor Spreading in the Tasman Sea: Nature, v. 243, no. 5408, p. 454-458.

Heikkilä, U., and von Blanckenburg, F., 2015, The global distribution of Holocene meteoric 10Be fluxes from atmospheric 630   models. Distribution maps for terrestrial Earth's surface applications, GFZ Data Services, doi.10.5880/GFZ.3.4.2015.001

Heisinger, B., Niedermayer, M., Hartmann, F., Korschinek, G., Nolte, E., Morteani, G., Neumaier, S., Petitjean, C., Kubik, P., and Synal, A., 1997, In-situ production of radionuclides at great depths: Nuclear Instruments and Methods in Physics Research Section B: Beam Interactions with Materials and Atoms, v. 123, no. 1-4, p. 341-346.

Helz, G. R., and Valette-Silver, N., 1992, Beryllium-10 in Chesapeake Bay sediments: An indicator of sediment provenance: 635   Estuarine, Coastal and Shelf Science, v. 34, no. 5, p. 459-469.

Higgins, N. C., Solomon, M., and Varne, R., 1985, The genesis of the Blue Tier Batholith, northeastern Tasmania, Australia: Lithos, v. 18, p. 129-149.

Jerie, K., Houshold, I., and Peters, D., 2003, Tasmania's river geomorphology: stream character and regional analysis: Nature Conservation Branch, DPIWE.

640   Jones, B., Chenhall, B., Debretsion, F., and Hutton, A., 2003, Geochemical comparisons between estuaries with non-industrialised and industrialised catchments: The Huon and Derwent River estuaries, Tasmania: Australian Journal of Earth Sciences, v. 50, no. 5, p. 653-667.

Jones, P. J., Williamson, G. J., Bowman, D. M. J. S., Lefroy, E. C., 2019, Mapping Tasmania's cultural landscapes: Using habitat suitability modelling of archaeological sites as a landscape history tool: Journal of Biogeography, v. 46, no. 11, p. 645   2570-2582.

Kidd, D., Malone, B., McBratney, A., Minasny, B., Odgers, N., Webb, M., and Searle, R., 2014, A new digital soil resource for Tasmania, Australia, in Proceedings 20th World Congress of Soil Science, p. 612-613.

Kidd, D., Webb, M., Malone, B., Minasny, B., and McBratney, A., 2015, 80-metre resolution 3D soil attribute maps for Tasmania, Australia: Soil Research, doi. 10.1071/SR14268.

650 Knighton, A., 1991, Channel bed adjustment along mine-affected rivers of northeast Tasmania: Geomorphology, v. 4, no. 3-4, p. 205-219.

Koehnken, L., 2001, North-east rivers environmental review: A review of Tasmanian environmental quality data to 2001: Supervising Scientist Report 168, Australian Government Department of Agriculture, Water and the Environment, pp. 64.

Kohl, C. P., and Nishiizumi, K., 1992, Chemical isolation of quartz for measurement of in-situ -produced cosmogenic nuclides:
655 Geochimica et Cosmochimica Acta, v. 56, no. 9, p. 3583-3587.

Kohn, B. P., Gleadow, A. J. W., Brown, R. W., Gallagher, K., O'Sullivan, P. B., and Foster, D. A., 2002, Shaping the Australian crust over the last 300 million years: Insights from fission track thermotectonic imaging and denudation studies of key terranes: Australian Journal of Earth Sciences, v. 49, no. 4, p. 697-717.

Kottek, M., Grieser, J., Beck, C., Rudolf, B., and Rubel, F., 2006, World map of the Köppen-Geiger climate classification
660 updated: Meteorologische Zeitschrift, v. 15, no. 3, p. 259-263.

Kragt, M. E., and Newham, L. T., 2009, Developing a water-quality model for the George catchment, Tasmania: Landscape Logic.

Lal, D., 1991, Cosmic ray labeling of erosion surfaces: in situ nuclide production rates and erosion models: Earth and Planetary Science Letters, v. 104, no. 2-4, p. 424-439.

665 Land-Tasmania, 2020, Fire History [of Tasmania]: Tasmania Department of Primary Industries, Water and Environment, Hobart, Tasmania, Australia, https://www.thelist.tas.gov.au/app/content/data/geo-meta-data-record?detailRecordUID=b94d4388-995d-416a-9844-a39de2798bed.

Lanyon, R., Varne, R., and Crawford, A. J., 1993, Tasmanian Tertiary basalts, the Balleny plume, and opening of the Tasman Sea (southwest Pacific Ocean): Geology, v. 21, no. 6, p. 555-558.

670 Mackintosh, A. N., Barrows, T. T., Colhoun, E. A., and Fifield, L. K., 2006, Exposure dating and glacial reconstruction at Mt. Field, Tasmania, Australia, identifies MIS 3 and MIS 2 glacial advances and climatic variability: Journal of Quaternary Science, v. 21, no. 4, p. 363-376.

Marshall, J. A., Roering, J. J., Gavin, D. G., and Granger, D. E., 2017, Late Quaternary climatic controls on erosion rates and geomorphic processes in western Oregon, USA: GSA Bulletin, v. 129, no. 5-6, p. 715-731.

675 Martin, J., and Cheetham, M., 2018, Final Report: Lower George River Investigation: Lower George Riverworks Trust.

Martin-Smith, K. M., and Vincent, A. C., 2005, Seahorse declines in the Derwent estuary, Tasmania in the absence of fishing pressure: Biological Conservation, v. 123, no. 4, p. 533-545.

Masarik, J., and Beer, J., 2009, An updated simulation of particle fluxes and cosmogenic nuclide production in the Earth's atmosphere: Journal of Geophysical Research: Atmospheres, v. 114, no. D11.

680 Matmon, A., Bierman, P., and Enzel, Y., 2002, Pattern and tempo of great escarpment erosion: Geology, v. 30, no. 12, p. 1135-1138.

McCarthy, T. S., and Groves, D. I., 1979, The Blue Tier Batholith, Northeastern Tasmania: Contributions to Mineralogy and Petrology, v. 71, no. 2, p. 193-209.

McDougall, I., and van der Lingen, G. J., 1974, Age of the rhyolites of the Lord Howe Rise and the evolution of the southwest
685 Pacific Ocean: Earth and Planetary Science Letters, v. 21, no. 2, p. 117-126.

McIntosh, P. D., Price, D. M., Eberhard, R., and Slee, A. J., 2009, Late Quaternary erosion events in lowland and mid-altitude Tasmania in relation to climate change and first human arrival: Quaternary Science Reviews, v. 28, no. 9, p. 850-872.

McKenny, C., and Shepherd, C., 1999, Ecological flow requirements for the George River: Report Series WRA 99/14, Department of Primary Industries, Water and Environment, Tasmania, pp. 31.

690 Mishra, A. K., Placzek, C., and Jones, R., 2019, Coupled influence of precipitation and vegetation on millennial-scale erosion rates derived from 10Be: PloS one, v. 14, no. 1, p. e0211325.

Mitchell, I. M., Crawford, C. M., and Rushton, M. J., 2000, Flat oyster (Ostrea angasi) growth and survival rates at Georges Bay, Tasmania (Australia): Aquaculture, v. 191, no. 4, p. 309-321.

Monaghan, M. C., Krishnaswami, S., and Turekian, K. K., 1986, The global-average production rate of10Be: Earth and
695 Planetary Science Letters, v. 76, no. 3, p. 279-287.

Mortimer, N., Campbell, H. J., Tulloch, A. J., King, P. R., Stagpoole, V. M., Wood, R. A., Rattenbury, M. S., Sutherland, R., Adams, C. J., Collot, J., and Seton, M., 2017, Zealandia: Earth's hidden continent: GSA Today, v. 27, p. 27-35.

Mount, R., Crawford, C., Veal, C., and White, C., 2005, Bringing back the bay: marine habitats and water quality in Georges Bay.

700   Murphy, R., Crawford, C., and Barmuta, L., 2003, Estuarine Health in Tasmania, Status and Indicators: Water Quality:
          Tasmanian Aquaculture and Fisheries Institute.
        Nanson, G. C., Von Krusenstierna, A., Bryant, E. A., and Renilson, M. R., 1994, Experimental measurements of river-bank
          erosion caused by boat-generated waves on the gordon river, Tasmania: Regulated Rivers: Research & Management, v.
          9, no. 1, p. 1-14.
705   Neilson, T. B., Schmidt, A. H., Bierman, P. R., Rood, D. H., and Sosa Gonzalez, V., 2017, Efficacy of in situ and meteoric
          10Be mixing in fluvial sediment collected from small catchments in China: Chemical Geology, v. 471, p. 119-130.
        Nichols, K. K., Bierman, P. R., and Rood, D. H., 2014, 10Be constrains the sediment sources and sediment yields to the Great
          Barrier Reef from the tropical Barron River catchment, Queensland, Australia: Geomorphology, v. 224, p. 102-110.
        Niemi, N. A., Oskin, M., Burbank, D. W., Heimsath, A. M., and Gabet, E. J., 2005, Effects of bedrock landslides on
710   cosmogenically determined erosion rates: Earth and Planetary Science Letters, v. 237, no. 3, p. 480-498.
        Nishiizumi, K., Imamura, M., Caffee, M. W., Southon, J. R., Finkel, R. C., and McAninch, J., 2007, Absolute calibration of
          10Be AMS standards: Nuclear Instruments and Methods in Physics Research Section B: Beam Interactions with Materials
          and Atoms, v. 258, no. 2, p. 403-413.
        Noe, G. B., Cashman, M. J., Skalak, K., Gellis, A., Hopkins, K. G., Moyer, D., Webber, J., Benthem, A., Maloney, K., and
715   Brakebill, J., 2020, Sediment dynamics and implications for management: State of the science from long-term research in
          the Chesapeake Bay watershed, USA: Wiley Interdisciplinary Reviews: Water, v. 7, no. 4, p. e1454.
        Persano, C., Stuart, F. M., Bishop, P., and Barfod, D. N., 2002, Apatite (U–Th)/He age constraints on the development of the
          Great Escarpment on the southeastern Australian passive margin: Earth and Planetary Science Letters, v. 200, no. 1, p.
          79-90.
720   Portenga, E. W., and Bierman, P. R., 2011, Understanding Earth's eroding surface with 10 Be: GSA Today, v. 21, no. 8, p. 4-
          10.
        Portenga, E. W., Bierman, P. R., Duncan, C., Corbett, L. B., Kehrwald, N. M., and Rood, D. H., 2015, Erosion rates of the
          Bhutanese Himalaya determined using in situ-produced 10Be: Geomorphology, v. 233, p. 112-126.
        Portenga, E. W., Bierman, P. R., Trodick, C. D., Jr., Greene, S. E., DeJong, B. D., Rood, D. H., and Pavich, M. J., 2019,
725   Erosion rates and sediment flux within the Potomac River basin quantified over millennial timescales using beryllium
          isotopes: GSA Bulletin, v. 131, no. 7-8, p. 1295-1311.
        Portenga, E. W., Bishop, P., Rood, D. H., and Bierman, P. R., 2017, Combining bulk sediment OSL and meteoric 10Be
          fingerprinting techniques to identify gully initiation sites and erosion depths: Journal of Geophysical Research: Earth
          Surface, v. 122, no. 2, p. 513-527.
730   Preston, K., 2012, Anchor tin mine, Tasmania: A century of struggle for profitability, Australasian Mining History Association,
          v. 10, p. 140–159.
        Puchol, N., Lavé, J., Lupker, M., Blard, P.-H., Gallo, F., and France-Lanord, C., 2014, Grain-size dependent concentration of
          cosmogenic 10Be and erosion dynamics in a landslide-dominated Himalayan watershed: Geomorphology, v. 224, p. 55-
          68.
735   Rahaman, W., Wittmann, H., and von Blanckenburg, F., 2017, Denudation rates and the degree of chemical weathering in the
          Ganga River basin from ratios of meteoric cosmogenic 10Be to stable 9Be: Earth and Planetary Science Letters, v. 469,
          p. 156-169.
        Reusser, L., Graly, J., Bierman, P., and Rood, D., 2010a, Calibrating a long-term meteoric 10Be accumulation rate in soil:
          Geophysical Research Letters, v. 37, no. 19.
740   Reusser, L. J., and Bierman, P. R., 2010, Using meteoric 10Be to track fluvial sand through the Waipaoa River basin, New
          Zealand: Geology, v. 38, no. 1, p. 47-50.
        Rosenkranz, R., Schildgen, T., Wittmann, H., and Spiegel, C., 2018, Coupling erosion and topographic development in the
          rainiest place on Earth: Reconstructing the Shillong Plateau uplift history with in-situ cosmogenic 10Be: Earth and
          Planetary Science Letters, v. 483, p. 39-51.
745   Schaller, M., Blanckenburg, F. v., Hovius, N., Veldkamp, A., van den Berg, M. W., and Kubik, P., 2004, Paleoerosion rates
          from cosmogenic 10Be in a 1.3 Ma terrace sequence: response of the River Meuse to changes in climate and rock uplift:
          The Journal of geology, v. 112, no. 2, p. 127-144.

Schaller, M., Ehlers, T., Lang, K. A., Schmid, M., and Fuentes-Espoz, J., 2018, Addressing the contribution of climate and vegetation cover on hillslope denudation, Chilean Coastal Cordillera (26–38 S): Earth and Planetary Science Letters, v. 489, p. 111-122.

Schaller, M., Ehlers, T., Stor, T., Torrent, J., Lobato, L., Christl, M., and Vockenhuber, C., 2016, Spatial and temporal variations in denudation rates derived from cosmogenic nuclides in four European fluvial terrace sequences: Geomorphology, v. 274, p. 180-192.

Schaller, M., von Blanckenburg, F., Hovius, N., and Kubik, P., 2001, Large-scale erosion rates from in situ-produced cosmogenic nuclides in European river sediments: Earth and Planetary Science Letters, v. 188, no. 3-4, p. 441-458.

Scherler, D., Bookhagen, B., and Strecker, M. R., 2014, Tectonic control on 10Be-derived erosion rates in the Garhwal Himalaya, India: Journal of Geophysical Research: Earth Surface, v. 119, no. 2, p. 83-105.

Schmidt, A. H., Gonzalez, V. S., Bierman, P. R., Neilson, T. B., and Rood, D. H., 2018, Agricultural land use doubled sediment loads in western China's rivers: Anthropocene, v. 21, p. 95-106.

Schmidt, A. H., Neilson, T. B., Bierman, P. R., Rood, D. H., Ouimet, W. B., and Sosa Gonzalez, V., 2016, Influence of topography and human activity on apparent in situ 10Be-derived erosion rates in Yunnan, SW China: Earth Surf. Dynam., v. 4, no. 4, p. 819-830.

Seen, A., Townsend, A., Atkinson, B., Ellison, J., Harrison, J., and Heijnis, H., 2004, Determining the History and Sources of Contaminants in Sediments in the Tamar Estuary, Tasmania, Using 210Pb Dating and Stable Pb Isotope Analyses: Environmental Chemistry, v. 1, no. 1, p. 49-54.

Seymour, D. B., Green, G. R., and Calver, C. R., 2006, The geology and mineral deposits of Tasmania: A summary: Mineral Resources Tasmania, https://www.mrt.tas.gov.au/products/publications/the_geology_and_mineral_deposits_of_tasmania_a_summary.

Siame, L., Angelier, J., Chen, R.-F., Godard, V., Derrieux, F., Bourlès, D., Braucher, R., Chang, K.-J., Chu, H.-T., and Lee, J.-C., 2011, Erosion rates in an active orogen (NE-Taiwan): A confrontation of cosmogenic measurements with river suspended loads: Quaternary Geochronology, v. 6, no. 2, p. 246-260.

Starke, J., Ehlers, T., and Schaller, M., 2017, Tectonic and climatic controls on the spatial distribution of denudation rates in Northern Chile (18 S to 23 S) determined from cosmogenic nuclides: Journal of Geophysical Research: Earth Surface, v. 122, no. 10, p. 1949-1971.

-, 2020, Latitudinal effect of vegetation on erosion rates identified along western South America: Science, v. 367, no. 6484, p. 1358-1361.

Stone, J., 1998, A Rapid Fusion Method for Separation of Beryllium-10 From Soils and Silicates: Geochimica et Cosmochimica Acta, v. 62, no. 3, p. 555-561.

Sutherland, R., King, P., and Wood, R., 2001, Tectonic evolution of Cretaceous rift basins in south-eastern Australia and New Zealand: Implications for exploration risk assessment, Petroleum Exploration Society of Australia Eastern Australasian Basins Symposium: Melbourne, Victoria, Australia.

Tomkins, K. M., Humphreys, G. S., Wilkinson, M. T., Fink, D., Hesse, P. P., Doerr, S. H., Shakesby, R. A., Wallbrink, P. J., and Blake, W. H., 2007, Contemporary versus long-term denudation along a passive plate margin: the role of extreme events: Earth Surface Processes and Landforms, v. 32, no. 7, p. 1013-1031.

Valette-Silver, J. N., Brown, L., Pavich, M., Klein, J., and Middleton, R., 1986, Detection of erosion events using 10Be profiles: example of the impact of agriculture on soil erosion in the Chesapeake Bay area (U.S.A.): Earth and Planetary Science Letters, v. 80, no. 1, p. 82-90.

van Dongen, R., Scherler, D., Wittmann, H., and von Blanckenburg, F., 2019, Cosmogenic 10Be in river sediment: where grain size matters and why: Earth Surf. Dynam., v. 7, no. 2, p. 393-410.

van Geen, A., Valette-Silver, N. J., Luoma, S. N., Fuller, C. C., Baskaran, M., Tera, F., and Klein, J., 1999, Constraints on the sedimentation history of San Francisco Bay from 14C and 10Be: Marine Chemistry, v. 64, no. 1, p. 29-38.

Vanacker, V., von Blanckenburg, F., Govers, G., Molina, A., Poesen, J., Deckers, J., and Kubik, P., 2007, Restoring dense vegetation can slow mountain erosion to near natural benchmark levels: Geology, v. 35, no. 4, p. 303-306.

Verdonschot, P., Spears, B., Feld, C., Brucet, S., Keizer-Vlek, H., Borja, A., Elliott, M., Kernan, M., and Johnson, R., 2013, A comparative review of recovery processes in rivers, lakes, estuarine and coastal waters: Hydrobiologia, v. 704, no. 1, p. 453-474.

von Blanckenburg, F., Bouchez, J., and Wittmann, H., 2012, Earth surface erosion and weathering from the 10Be (meteoric)/9Be ratio: Earth and Planetary Science Letters, v. 351-352, p. 295-305.

Weissel, J. K., and Hayes, D. E., 1977, Evolution of the Tasman Sea reappraised: Earth and Planetary Science Letters, v. 36, no. 1, p. 77-84.

Willenbring, J. K., and von Blanckenburg, F., 2010, Meteoric cosmogenic Beryllium-10 adsorbed to river sediment and soil: Applications for Earth-surface dynamics: Earth-Science Reviews, v. 98, no. 1, p. 105-122.

Wilson, C. J., 1999, Effects of logging and fire on runoff and erosion on highly erodible granitic soils in Tasmania: Water Resources Research, v. 35, no. 11, p. 3531-3546.

Wittmann, H., Malusà, M. G., Resentini, A., Garzanti, E., and Niedermann, S., 2016, The cosmogenic record of mountain erosion transmitted across a foreland basin: Source-to-sink analysis of in situ 10Be, 26Al and 21Ne in sediment of the Po river catchment: Earth and Planetary Science Letters, v. 452, p. 258-271.

Wittmann, H., Oelze, M., Gaillardet, J., Garzanti, E., and von Blanckenburg, F., 2020, A global rate of denudation from cosmogenic nuclides in the Earth's largest rivers: Earth-Science Reviews, v. 204, p. 103147.

Wittmann, H., von Blanckenburg, F., Bouchez, J., Dannhaus, N., Naumann, R., Christl, M., and Gaillardet, J., 2012, The dependence of meteoric 10Be concentrations on particle size in Amazon River bed sediment and the extraction of reactive 10Be/9Be ratios: Chemical Geology, v. 318-319, p. 126-138.

Wittmann, H., von Blanckenburg, F., Dannhaus, N., Bouchez, J., Gaillardet, J., Guyot, J. L., Maurice, L., Roig, H., Filizola, N., and Christl, M., 2015, A test of the cosmogenic 10Be(meteoric)/9Be proxy for simultaneously determining basin-wide erosion rates, denudation rates, and the degree of weathering in the Amazon basin: Journal of Geophysical Research: Earth Surface, v. 120, no. 12, p. 2498-2528.

Wittmann, H., von Blanckenburg, F., Guyot, J.-L., Maurice, L., and Kubik, P., 2011, Quantifying sediment discharge from the Bolivian Andes into the Beni foreland basin from cosmogenic 10Be-derived denudation rates: Revista Brasileira de Geociências, v. 41, no. 4, p. 629-641.

Wittmann, H., von Blanckenburg, F., Guyot, J. L., Maurice, L., and Kubik, P. W., 2009, From source to sink: Preserving the cosmogenic 10Be-derived denudation rate signal of the Bolivian Andes in sediment of the Beni and Mamoré foreland basins: Earth and Planetary Science Letters, v. 288, no. 3, p. 463-474.

Wolanski, E., and Ducrotoy, J.-P., 2014, Estuaries of Australia in 2050 and beyond–A synthesis, Estuaries of Australia in 2050 and beyond, Springer, p. 1-13.

Yanites, B. J., Tucker, G. E., and Anderson, R. S., 2009, Numerical and analytical models of cosmogenic radionuclide dynamics in landslide-dominated drainage basins: Journal of Geophysical Research: Earth Surface, v. 114, no. F1.